RESOLUTION STUDY ON WAVELETS BOTH IN TEMPORAL AND SPECTRAL DOMAIN

A Thesis

Presented to

the Faculty of the Department of Earth and Atmospheric Sciences

University of Houston

In Partial Fulfillment

of the Requirements for the Degree

Master of Science

By

Mingyong Chen

April 2012

RESOLUTION STUDY ON WAVELETS BOTH IN TEMPORAL AND SPECTRAL DOMAIN

Mingyong Chen

APPROVED:

Dr. John P. Castagna, Chairman
Department of Earth and Atmospheric Sciences

Dr. Christopher L. Liner
Department of Earth and Atmospheric Sciences

Dr. Don Kouri
Department of Chemistry

Dr. Oleg Portniaguine
Computational Geophysics, LLC

Dean, College of Natural Sciences and Mathematics

Acknowledgements

I am heartily thankful to my supervisor, Dr. John P. Castagna, PhD, for his insightful suggestions on my research, for his guidance throughout the Masters program, and for his willingness to share the wisdom of life with me. I would like to thank the rest of my thesis committee, Dr. Christopher L. Liner, PhD, Dr. Donald Kouri, PhD, and Dr. Oleg Portniaguine, PhD, for their encouragement and invaluable input to my work. I would like to thank my friends, who are always willing to help and discuss tough questions I encountered. Last but not the least, I would like to thank my family for supporting me and believing in me as always.

RESOLUTION STUDY ON WAVELETS BOTH IN TEMPORAL AND SPECTRAL DOMAIN

An Abstract of a Thesis

Presented to

the Faculty of the Department of Earth and Atmospheric Sciences

University of Houston

In Partial Fulfillment

of the Requirements for the Degree

Master of Science

By

Mingyong Chen

April 2012

Abstract

An improved version of Matching Pursuit Decomposition (MPD), called Fractional Matching Pursuit Decomposition (FMPD), which can solve the lateral instability problem caused by conventional Matching Pursuit Decomposition, is proposed. On synthetic data, including a wedge model and the Dickman field real dataset, FMPD results show better lateral continuity among all the applications than conventional MPD.

In pursuing better resolution in spectral decomposition, the conventional uncertainty principle is not adequate for application purpose. An alternative definition of uncertainty principle, which could clearly and quantitatively define combined temporal and spectral resolution concerned in spectral decomposition, is presented. According to this, complex uncertainty principle, the lowest limit is still valid if we consider zero mean condition into wavelet selection.

Contents

List of Figures

Chapter 1

Introduction

Spectral decomposition has drawn people's attention in exploration geophysics since Partyka et al. [1999] explicitly revealed the value of it in reservoir characterization. Frequency representation of seismic data provided us a new perspective to process and interpret, which frequently excavated detailed information that was buried in time representation. The value of this new method was validated when more people applied it to the real data. Over a decade's exploration in this subject, spectral decomposition has proved to be useful in many ways which significantly reduce the chance of misinterpretation and support the drilling plans [Johann et al., 2003, Cuesta et al., 2009]. Spectral decomposition is extremely useful in channel delineation [Partyka et al., 1999, Sinha et al., 2005, Liu and Marfurt, 2007, Guo et al., 2009, Verma et al., 2009, Li et al., 2010]; fault detection [Alam and Taylor, 2006, Pokhriyal and Dotiwala, 2007]; subtle discontinuities detection [Matos et al., 2009, Li et al., 2010]; hydrocarbon indication [Burnett et al., 2003, Castagna et al., 2003, Hernandez and Castagna, 2004, Fahmy et al., 2005, Guo et al., 2006, Wang, 2007, Tai et al., 2009,

Li et al., 2011]; gas and brine separation, i.e. fluid property discrimination [Montoya et al., 2005, Chen et al., 2006, Zhao et al., 2006, Deng et al., 2007]; thickness estimation [Barnes et al., 2004, Marfurt and Kirlin, 2001]; general reservoir characterization [Li and Zhang, 2008, Guo et al., 2009, Zhang et al., 2009]; dispersion analysis and Q estimation [Odebeatu et al., 2006, Singleton et al., 2006]; automatic first break detection [Liao et al., 2011]; interpolation between traces [Ozbek et al., 2009]; hidden structural and stratigraphic features detection [Peyton et al., 1998, Johann et al., 2003, Giroldi and Alegria, 2005, Spitzer et al., 2007, Sierra et al., 2009]; thinbed reflectivity inversion [Chopra et al., 2006, 2007, 2009]. It is fair to say that further investigation of spectral decomposition would broaden its value in exploration geophysics other than what have described above.

The general idea of spectral decomposition is to transform a seismic trace from 1-D time series to a 2-D panel covering both time and frequency domains at the same time. In practice, time frequency analysis often reveals more information than is obvious from broad band dataset. However, many similar methods can successfully decompose the seismic data into frequency representation. By extracting frequency attributes out of the dataset, we can characterize the reservoir more accurately. The first application of spectral decomposition in 3D dataset using Discrete Fourier Transform(DFT) was by Partyka et al. [1999]. It was a giant success in reservoir characterization [Gridley and Partyka, 1997, Partyka et al., 1999, Johann et al., 2003, Giroldi and Alegria, 2005, Montoya et al., 2005]. In order to overcome the fixed resolution problem of DFT, Continuous Wavelet Transform(CWT) was applied [Alam and Taylor, 2006, Matos and Marfurt, 2008, Sierra et al., 2009, Sinha

et al., 2009]. An alternative method called Matching Pursuit Decomposition(MPD) [Castagna et al., 2003, Fahmy et al., 2005, Geerdes and Young, 2005, Zhao et al., 2006, Bradford and Wu, 2007, Wang, 2007, Liu and Marfurt, 2007, Ozbek et al., 2009] was applied and showed better resolution than DFT and CWT. In general, those three methods are quite similar to each other, each has its own advantages and each does sufficient jobs on spectral decomposition. However, comparison between those three methods [Chakraborty and Okaya, 1995] shows that MPD has best combined resolution. Castagna et al. [2003] had also showed time frequency maps of these three methods on synthetic data. Thorough comparison between CWT and MPD on real data application can be found in Puryear's paper (2008) [Puryear et al., 2008]. Other methods like Wigner-Ville Distribution (WVD) [Guo et al., 2006, Li et al., 2010], smoothed WVD [Li and Zhang, 2008], S transform [Miao et al., 2007] are also actively studied.

In my thesis, I limit my study to DFT, CWT, and MPD. There is an improvement on MPD, I called it fractional MPD, which can solve the lateral instability problem caused by conventional MPD. We are always trying to pursue better resolution on spectral decomposition, not only temporally but also spectrally. Since wavelet based spectral decomposition methods have exhibited its value in real data applications, it is needed to examine what factor really controls the power of resolution. It is generally said that time spread of waveform and bandwidth of spectrum cannot be made arbitrarily small simultaneously. And there is a lowest limit of 1/2 derived from mathematical definition. However careful examination upon uncertainty principle suggests that, the conventional uncertainty product is not accurate to characterize

the resolution on spectral decomposition. Instead, we should use complex uncertainty principle which is comprehensively described in chapter 4.

Chapter 2

Basic Theory—Time Frequency Analysis

2.1 Fourier Transform (FT)

Mathematical theory of modern time frequency analysis is based on the Fourier Transform. This seemingly simple and well-known transform is named after Joseph Fourier, a 19th century Franch scientist.

In 1807, Joseph Fourier was fascinated about the behavior of heat. He was in struggle of finding the solution to the function of heat transmission. The trickiness of this problem is when hot and cold objectives were put into contact, the discontinuity in temperature arose. Joseph Fourier's remarkable idea of the solution is to use a series of continuous functions to represent the discontinuous function, which seems absurd at that time of understanding, turns out to be the most powerful scientific method that had been discovered. We could also view the Fourier Transform as decomposing

the function/signal using the expansion functions of sine and cosine function/signal at different values of parameter, which we call that parameter frequency.

The first application of Fourier Transform was almost 60 years after the discovery of this method which is a tremendous loss of 60 years. However, by that application we could quantitatively differentiate light with different colors by frequency. Even though the value of Fourier Transform is tremendous, there are limitations in it. One major assumption is that the signal is considered to be stationary for Fourier Transform to be absolutely correct. Stationary signals are constant in their statistical parameters over time. However, seismic signals are non-stationary signals begin with non-stationary source. Also truncated signals with finite time length are always non-stationary. Primary solution was using Short Window Fourier Transform when they were dealing with speeches, which is totally applicable in seismic analysis.

2.2 Short Time Fourier Transform (STFT)

Since we could view Fourier Transform as the summation of a series of sine and cosine waves at different frequencies, it is convenient for us to write the transform as followed:

$$S(t) = \int_{-\infty}^{\infty} A(\omega)\cos(\omega t)d\omega + \int_{-\infty}^{\infty} B(\omega)\sin(\omega t)d\omega \tag{2.1}$$

In this case, STFT could be written as followed:

$$S(t)w(t-\tau) = \int_{t_1}^{t_2} w(t-\tau)A(\omega)\cos(\omega t)d\omega + \int_{t_1}^{t_2} w(t-\tau)B(\omega)\sin(\omega t)d\omega \tag{2.2}$$

The assumption for STFT was that truncated signals are stationary, which is approximated true for an efficiently small window. Due to the Uncertainty Principle(UP),

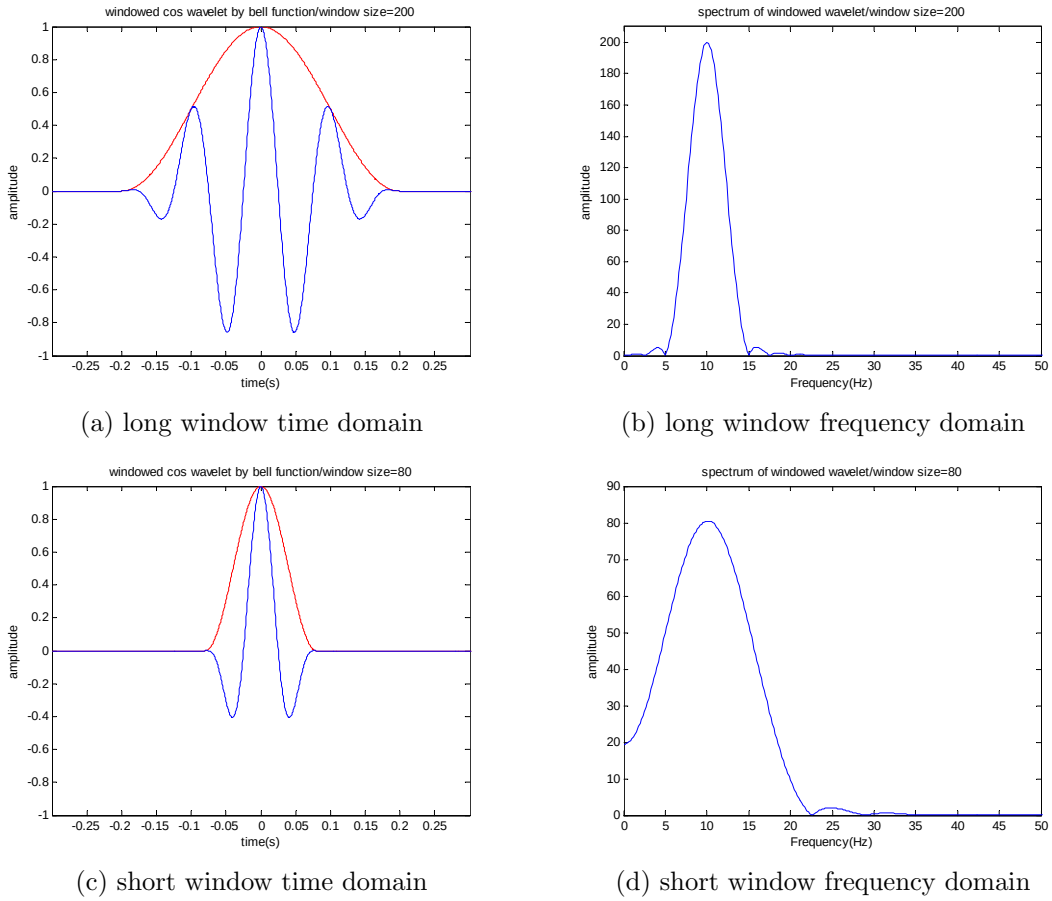

(a) long window time domain

(b) long window frequency domain

(c) short window time domain

(d) short window frequency domain

Figure 2.1: Illustration of uncertainty principle

which states that there is a limitation combined the resolution in temporal and spectral domain, we cannot arbitrarily obtain optimal resolution both in time and spectrum as illustrated in Figure 2.1.

Therefore, once the window for STFT was chosen, we faced a fixed resolution through the whole seismic trace. However, in reality, long window is preferred if that is sufficient enough to represent the signal, which could also decrease consummation of time in computation. And short window is preferred where there is dominated by high frequency signals. In general, we tend to adjust the window sizes throughout

the trace. To accomplish this expectation, we could use Wavelet Transform(WT) which has adjusted resolution.

2.3 Wavelet Transform(WT)

$$S(a,b) = \frac{1}{\sqrt{|a|}} \int_{-\infty}^{\infty} S(t)\psi^{\star}\left(\frac{t-b}{a}\right) dt \tag{2.3}$$

In a simple way, WT can be considered as cross-correlating adjusted mother wavelet with seismic trace and laying out the correlation coefficient on the time scale map. However, we can always transform scale to frequency and get a time frequency map. There are two major categories for WT when we computed it. They are:

- Continuous Wavelet Transform (CWT): which uses a sliding window through the trace with overlapping.
- Discrete Wavelet Transform (DWT): which uses a series of window segments without overlapping.

Note that Morlet wavelets do not constitute orthogonal basis. Because of overlapping, we have plenty of redundant information. Even in DWT analysis, Morlet wavelet is only approximately orthogonal since we have infinite extended tails of Gaussian. There are orthogonal wavelets to be used in WT analysis such as Daubechies [Daubechies, 1990]. Between the choice of weird shape of wavelet like Daubechies and good-looking shape of wavelet like Morlet, I vote for Morlet for the reason that I believe the beauty of the universe is simplicity. And approximately orthogonal Morlet wavelet is enough. If we use Morlet wavelet as the mother wavelet, we could consider Morlet wavelet

transform as STFT with a Gaussian window. Their major difference is whether the shape of the window can be adjusted or not.

Mathematically, we tend to decompose signals into sine and cosine waves. Because these waves are beautiful. They are periodic. Moreover, complex analysis is easier in some ways. There is a big connection between complex waves and Fourier waves which is Euler Equation:

$$e^{-i\theta t} = \cos(\theta t) + i * \sin(\theta t) \tag{2.4}$$

Special case of Euler Equation:

$$e^{i\pi} + 1 = 0 \tag{2.5}$$

This special case, combining natural logarithm e, circumference ratio π, imaginary unit i, integer unit 1 and the greatest 0, is the most beautiful function in the mathematical world in my and perhaps many others' perspective. This equation is also valued as "God made equation" by mathematicians. While geophysically, what we are dealing with is the convolution of impulse and Earth medium. Instead of using truncated Fourier waves, how about we use some impulse-like waves to represent seismic signals? Followed by this intuitive, Matching Pursuit was applied to decompose seismic signals into impulse-like wavelets, Ricker wavelets.

Chapter 3

Matching Pursuit Decomposition

3.1 Matching Pursuit (MP)

Matching Pursuit is a statistical regression method. Mallat and Zhang [1993] had clear demonstrated what is Matching Pursuit and all the mathematical concerns about it. One statistical paper by Friedman [Friedman et al., 2000] had pointed out that Matching Pursuit used by Mallat and Zhang was a greedy approach of a more sophisticated method called additive model.

$$S(t) = \sum_{n=0}^{\infty} a_n g_{\gamma n}(t) \tag{3.1}$$

Whether this additive model will reveal more information from seismic data or not is left to be explored. However, this greedy approach has a great advantage in time consummation. In Chapter two, we will discuss more about matching pursuit and some improvements of it.

The objective of matching pursuit is to reconstruct the original signal with the combination of best matched wavelets from a pool of wavelet dictionary. After that, we distribute the spectra of matched wavelets along the envelop of the matched wavelet in time frequency map to get the energy distribution of the signal. Figure 3.1 has explicitly described the procedure of Matching Pursuit Decomposition (MPD) algorithm.

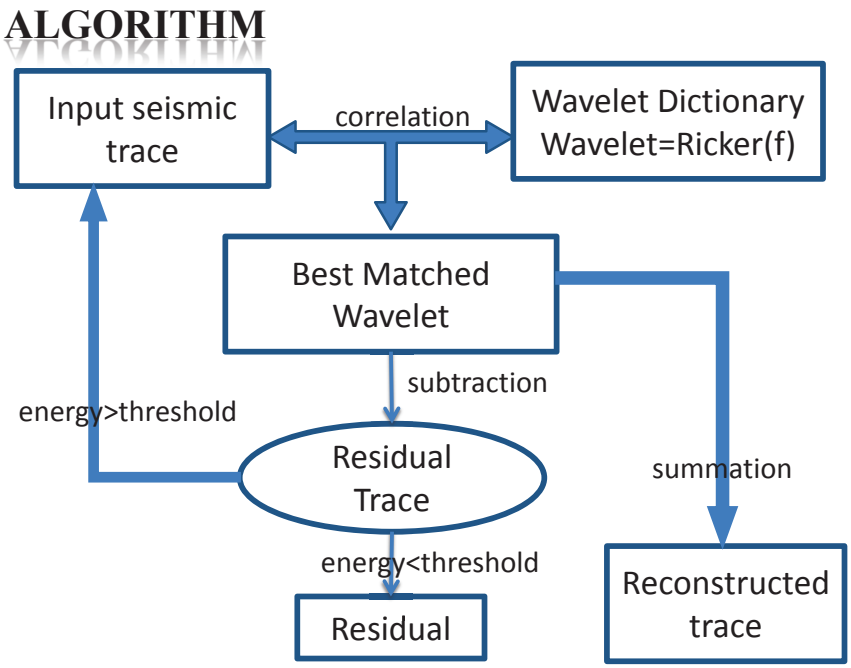

Figure 3.1: Algorithm of conventional MPD

3.2 Criteria for Wavelets

The algorithm behind MP is simple. However the choice of wavelet dictionary is not. Same as in WT, for efficiency reasons, there are some criteria to choose wavelets as the dictionary.

3.2.1 Compact Support

$$\int_{-\infty}^{\infty} |\psi(t)|\, dt < \infty \quad and \quad \int_{-\infty}^{\infty} |\psi(t)|^2\, dt < \infty \tag{3.2}$$

The reason for compacted wavelet is easy to imagine compared to the choice of the window length. Compacted wavelet is just like a window to extract the segment of the signal to be analyzed.

3.2.2 Zero Mean

$$\int_{-\infty}^{\infty} \psi(t) dt = 0 \tag{3.3}$$

Zero mean condition is crucial in reality. We are supposed to have no information from the real signal at 0Hz which means $\hat{\psi}(\omega)|_{\omega=0} = 0$, where $\hat{\psi}(\omega) = FT(\psi(t))$.

3.2.3 Energy Normalization

$$\int_{-\infty}^{\infty} |\psi(t)|^2\, dt = 1 \tag{3.4}$$

Normalized wavelets are convenient for computation. If we used un-normalized wavelets, the cross-correlated coefficient would have to be adjusted by normalization. For physical reasons, I prefer using energy normalization instead of other means like absolute normalization.

Besides these criteria for wavelet choice, we also need to consider the parameters of the wavelet dictionary. Apart from frequency which is essential parameter in time

frequency analysis, phase parameter is somewhat important. And phase is changing through the propagation of waves. Therefore, should we consider phase into our analysis? How much difference would it make if we consider phase? In order to seek answers to these questions, we compared three kinds of Matching Pursuit Decomposition (MPD).

3.3 Three MPDs

3.3.1 Conventional MPD

Wavelet dictionary:

$$Wavelet = Ricker(f) \tag{3.5}$$

The procedure of conventional MPD was shown in the Figure 3.1. The dictionary used in this method is wavelets at different frequencies.

3.3.2 Phase MPD

Wavelet dictionary:

$$Wavelet = Ricker(f, \varphi) \tag{3.6}$$

The procedure of phase MPD is also the same as the conventional MPD. The only difference between them is the wavelets used in this method are not only at different frequencies but also at difference phase. By adding a phase parameter, we consequently expand the amount of the wavelets in the dictionary which results in longer computing time.

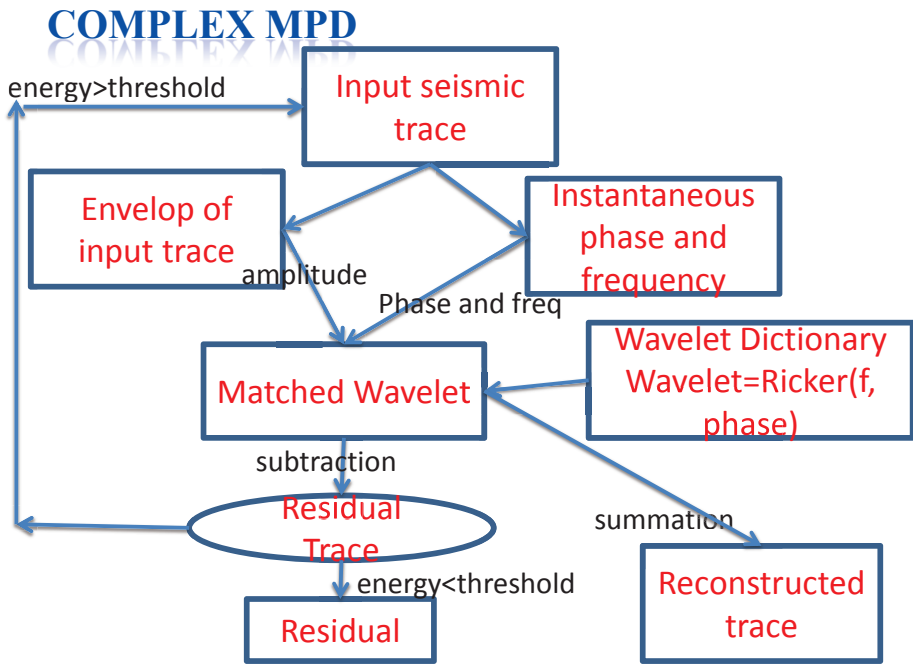

Figure 3.2: Algorithm of complex MPD

3.3.3 Complex MPD

Complex MPD is still in progress but shows promising results. Instead of cross-correlate wavelets with seismic signals, we extract frequency and phase information directly from seismic signals. By using the relationship between instantaneous frequency and dominant frequency of Ricker wavelet, we could construct the complex Ricker wavelet, and subtract the constructed wavelet every iteration until the energy of the residual trace is low enough. The algorithm is illustrated in Figure 3.2.

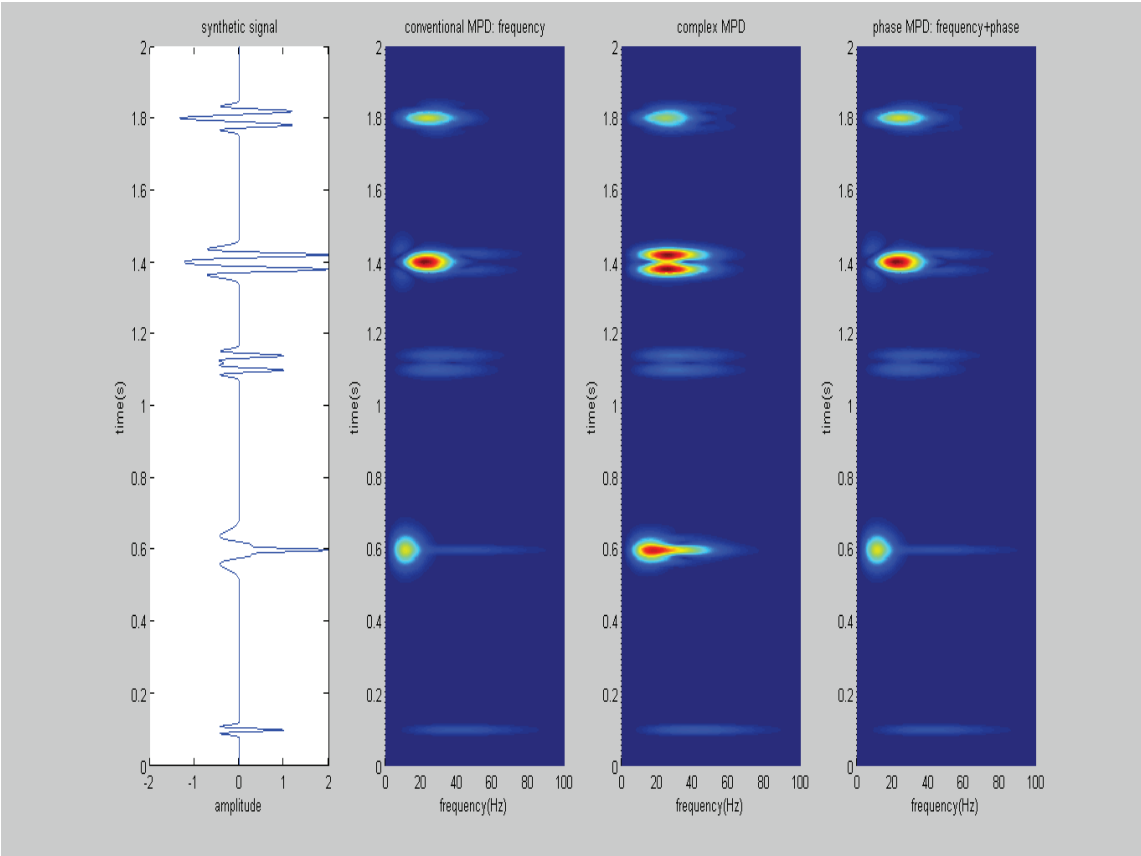

Figure 3.3: Three MPDs on synthetic trace

3.4 Synthetic Results of Three MPDs

I applied all three MPDs on synthetic trace I generated similar to the synthetic trace in Castagna et al. [2003]. Due to the synthetic trace was generated by convolving zero phase wavelets with reflectivity, we are expecting similar results of conventional MPD and phase MPD, which is exactly shown in the Figure 3.3. And we can see that complex MPD is good at resolving separate event like a 2nd event, while the other two MPDs are good at resolving overlayed event like a 4th event.

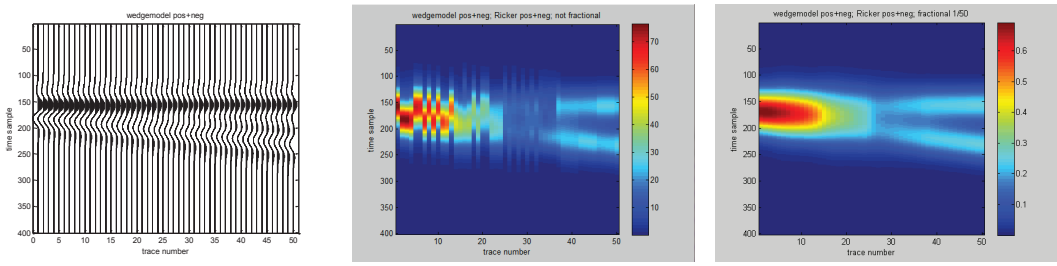

(a) wedge model 1

(b) frequency slice of MPD results

(c) frequency slice of FMPD results

Figure 3.4: Frequency slice of conventional MPD versus fractional MPD results on wedge model with odd RC

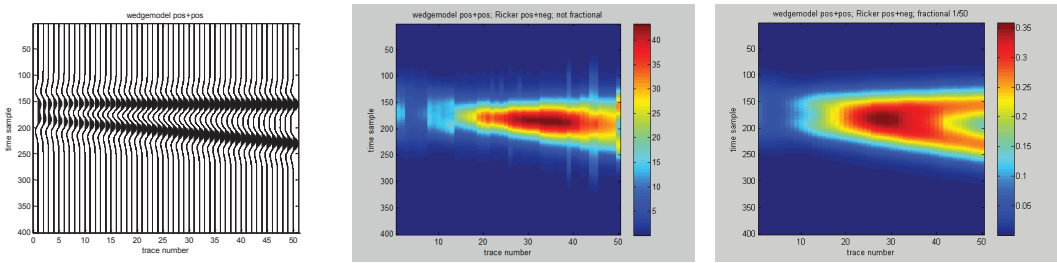

(a) wedge model 2

(b) frequency slice of MPD results

(c) frequency slice of FMPD results

Figure 3.5: Frequency slice of conventional MPD versus fractional MPD results on wedge model with even RC

3.5 Solution for Instability—Fractional MPD

When we applied conventional MPD on 2D profile, and look at the frequency slice of the results, we can see clear lateral instability. We found out that by subtracting only a portion of the coefficient, we can solve the amplitude inconsistency problem. Comparison between MPD and FMPD on a wedge model at a vertical section is shown in Figure 3.4, Figure 3.5, and Figure 3.6.

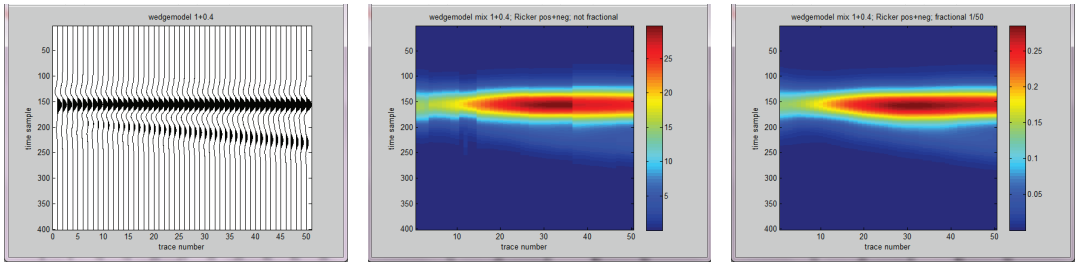

(a) wedge model 3

(b) frequency slice of MPD results

(c) frequency slice of FMPD results

Figure 3.6: Frequency slice of conventional MPD versus fractional MPD results on wedge model with mix RC

3.6 Reason for Lateral Instability

We suspected that the reason for lateral instability was because of orthogonality. Due to the Ricker wavelet is not orthogonal, the path it chose to find the bested matched wavelet varies. In another way, conventional MPD using non-orthogonal wavelets as the dictionary is path dependent. If we use approximately orthogonal wavelets like Morlet wavelet, the difference between MPD spectra and FMPD spectra is small. The instability occurred when the trace had two identical reflections. Conventional MPD couldn't decide which one to be subtracted first. However, fractional MPD beautifully solves the problem. The speculation is reinforced by the comparison shown in Figure 3.7:

And more comparison between MPD and FMPD on vertical sections and timeslices is presented in Appendix A and Appendix B.

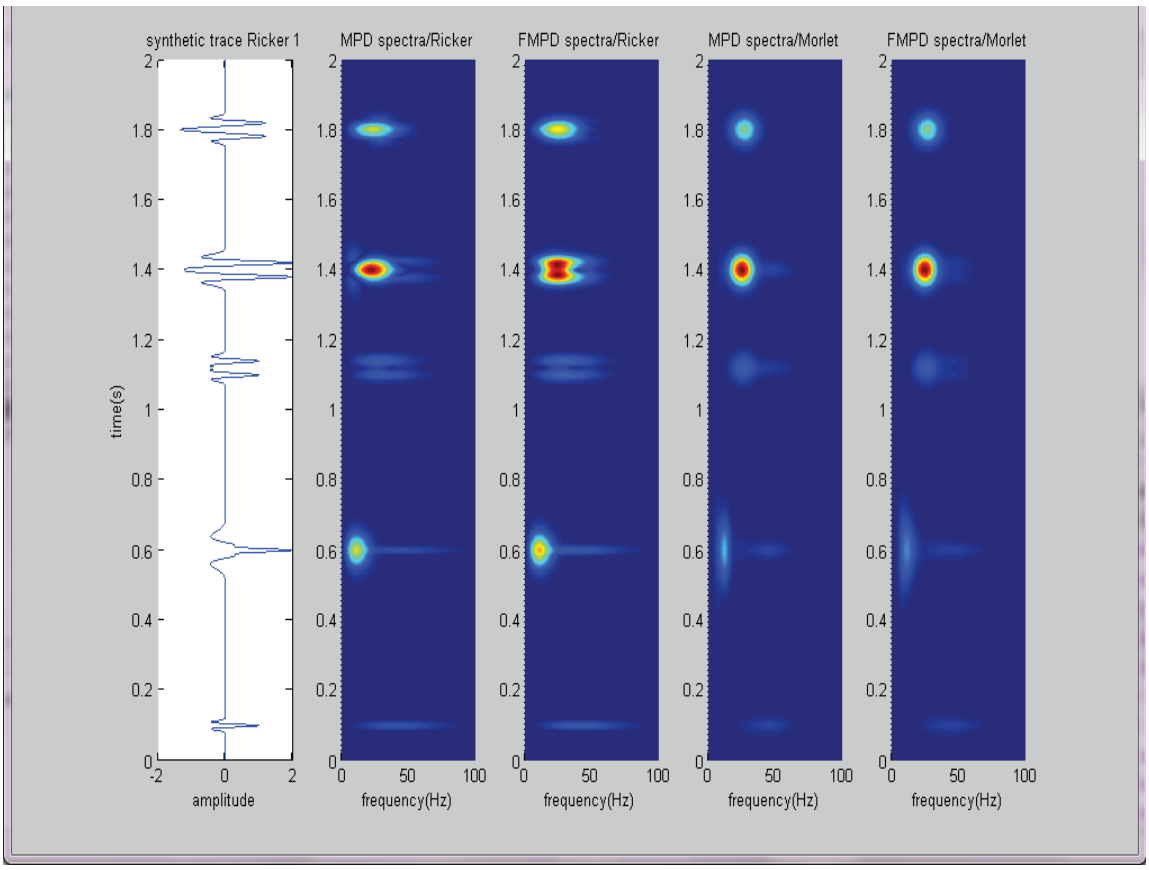

Figure 3.7: Reason for lateral instability

Chapter 4

Uncertainty Principle

4.1 A World Full of Uncertainties

Quantum mechanics provides us a new perspective to redefine our world. The Heisenberg's Uncertainty Principle strikes us the knowledge that we cannot arbitrarily determine precisely the position and the momentum of certain particles simultaneously. Our world is all about probabilities. Analogously, we discover some kind of similar relationship between temporal and spectral resolution. However, unlike quantum mechanics, in time frequency analysis, there is nothing uncertain about temporal or spectral resolution. We can only have a wide waveform with a narrow spectrum or a narrow waveform with a wide spectrum, which says that the combined resolution in time and frequency domain is constant. In order to get better resolution in one domain, we have to sacrifice the other.

4.2 Motivation for Resolution Pursuit

A window is a wavelet and vice versa. Spectral decomposition methods, such as Short Time Fourier Transform (STFT), Wavelet Transform (WT), and Matching Pursuit Decomposition (MPD), all encounter issues of windows or wavelets. The problem of uncertainty principle is inevitably attached to spectral decomposition analysis. While we are pursuing better time resolution for better structure imaging, we want better frequency resolution, which can help us in differentiating various geological features [Castagna et al., 2003]. The research on uncertainty product of various kinds of wavelets is a good way to pursue better resolution on spectral analysis. In this chapter, we compare Ricker wavelet, Morlet wavelet, mu-wavelets, and pseudo-mu-wavelets by calculating their uncertainty product. We found out that the mathematical definition of uncertainty principle is not accurate for our purpose, pursuing better resolution on spectral decomposition. We come up with a new definition of calculating uncertainty product, which is called complex uncertainty product, serves as a practical representation.

4.3 Mathematical Definition of Uncertainty Principle

A commonly accepted uncertainty product was defined using standard deviation. It is by this definition that uncertainty product has been proved to have the lowest limit 1/2. Let's see how it is defined. We consider a pair of signals defined by Fourier

Transform(FT):

$$S(\omega) = FT(S(t)) = \int_{-\infty}^{\infty} S(t)e^{-i\omega t}dt \tag{4.1}$$

We consider unit energy signal here. The signal can always be converted to have unit energy with following equations:

$$S(t)_{after} = \frac{S(t)_{before}}{\sqrt{\int_{-\infty}^{\infty} |S(t)_{before}|^2 dt}} \tag{4.2}$$

and

$$S(\omega)_{after} = \frac{S(\omega)_{before}}{\sqrt{\int_{-\infty}^{\infty} |S(\omega)_{before}|^2 d\omega}} \tag{4.3}$$

After conversion, the energy of the signal resembles a probability function.

$$E = \int_{-\infty}^{\infty} |S(t)|^2 dt = \int_{-\infty}^{\infty} |S(\omega)|^2 d\omega = \int_{-\infty}^{\infty} P(A)dA = 1 \tag{4.4}$$

We can then calculate mean value of time and frequency using following equations:

$$< t >= \int_{-\infty}^{\infty} t|S(t)|^2 dt \tag{4.5}$$

and

$$< \omega >= \int_{-\infty}^{\infty} \omega|S(\omega)|^2 d\omega \tag{4.6}$$

The variance (square of standard deviation) of time and frequency can be expressed as followed:

$$\sigma_t^2 = \int_{-\infty}^{\infty} (t- < t >)^2 |S(t)|^2 dt \tag{4.7}$$

and

$$\sigma_\omega^2 = \int_{-\infty}^{\infty} (\omega- < \omega >)^2 |S(\omega)|^2 d\omega \tag{4.8}$$

Therefore, uncertainty product(UP) can be defined as the combination of σ_t and σ_ω:

$$UP = \sigma_t * \sigma_\omega \geq 1/2 \tag{4.9}$$

4.4 Lowest Limit of UP—Gaussian

Proved by Cohen in his book time frequency analysis [Cohen, 1994], Gaussian wavelet has the lowest uncertainty product by definition using standard deviation. The proof procedure is rewritten as followed: First we prove the uncertainty product has the lowest limit 1/2. We assume a signal:

$$S(t) = A(t)e^{-i\varphi(t)} \tag{4.10}$$

which satisfies,

$$\int_{-\infty}^{\infty} |S(t)|^2 \, dt = 1 \implies \int_{-\infty}^{\infty} A(t)^2 dt = 1 \tag{4.11}$$

This derivation is valid for signals have zero mean time and zero mean frequency. However, presented by Cohen [Cohen, 1994], every signal can always be shifted to have zero mean time and zero mean frequency by following equation:

$$s_{new}(t) = e^{-i<\omega>(t+<t>)} s_{old}(t+ < t >) \tag{4.12}$$

Therefore, we have the new signal with zero mean time $< t >= 0$ and zero mean frequency $< \omega >= 0$. From that, we deduce,

$$\sigma_t^2 = \int_{-\infty}^{\infty} t^2 |S(t)|^2 dt \tag{4.13}$$

and

$$\sigma_\omega^2 = \int_{-\infty}^{\infty} \omega^2 |S(\omega)|^2 d\omega = \int_{-\infty}^{\infty} |S'(t)|^2 dt \tag{4.14}$$

The square of uncertainty product can be represented as,

$$\sigma_t^2 \sigma_\omega^2 = \int_{-\infty}^{\infty} t^2 |s(t)|^2 dt \times \int_{-\infty}^{\infty} |'(t)|^2 dt \tag{4.15}$$

Schwarz Inequality states,

$$\int |f(x)|^2 dx \int |g(x)|^2 dx \geq |f^*(x)g(x)dx|^2 \tag{4.16}$$

where, $f^*(x)$ is the complex conjugate of $f(x)$.

Therefore, if we take $ts(t)$ as f and $s'(t)$ as g, we derive Eq. 4.15 to the following and get the lowest limit,

$$\begin{aligned}
\sigma_t^2 \sigma_\omega^2 &\geq \left| \int ts^*(t)s'(t)dt \right|^2 \\
&= \left| \int (tA'A + it\varphi' A^2)dt \right|^2 \\
&= \left| \int (\frac{1}{2}\frac{d}{dt}tA^2 - \frac{1}{2}A^2 + it\varphi'(A^2))dt \right|^2 \\
&= \left| -\frac{1}{2} + iCov_{t\omega} \right|^2 \\
&= \frac{1}{4} + Cov_{t\omega}^2 \\
&\geq \frac{1}{4}
\end{aligned} \tag{4.17}$$

where, $Cov_{tw} =< t\varphi'(t) > - < t >< \omega >=< t\varphi'(t) >$, since $< t >< \omega >= 0$. If above those two inequalities were satisfied, Schwarz Inequality equals if only f is proportional to g which gives us,

$$-c * t * s(t) = s'(t) \tag{4.18}$$

from that, we can derive,

$$s(t) = e^{-(c_r + ic_i)t^2/2} \tag{4.19}$$

and we have condition for the other inequality to be equal,

$$Cov_{tw} =< t\varphi'(t) >= \int t\varphi' |s(t)|^2)dt = 0 \tag{4.20}$$

Let's put Eq. 4.19 into Eq. 4.20 and get,

$$\begin{aligned} Cov_{tw} &= \int t\varphi'|s(t)|^2)dt \\ &= -\int tc_i t|s(t)|^2)dt \\ &= -c_i \int t^2 e^{-c_r t^2})dt \\ &= 0 \qquad (4.21) \\ \Longrightarrow c_i &= 0 \qquad (4.22) \end{aligned}$$

Put Eq. 4.22 back into Eq. 4.19, we obtain the wavelet which has the lowest limit which is Gaussian wavelet.

$$s(t) = (\alpha/\pi)^{1/4} e^{-\alpha t^2/2} \qquad (4.23)$$

where $(\alpha/\pi)^{1/4}$ is the normalization coefficient.

4.5 Results of Conventional Uncertainty Product

Algorithm for calculating uncertainty product of different wavelets is based on the mathematical definition. Figure 4.1 has clearly explained the procedures. The following figure illustrates the last part of the procedure, The standard deviations of various wavelets are presented in the Appendix A. We compared the conventional UP of different wavelets in the Figure 4.3. We found out that uncertainty product of wavelet is independent of frequency.

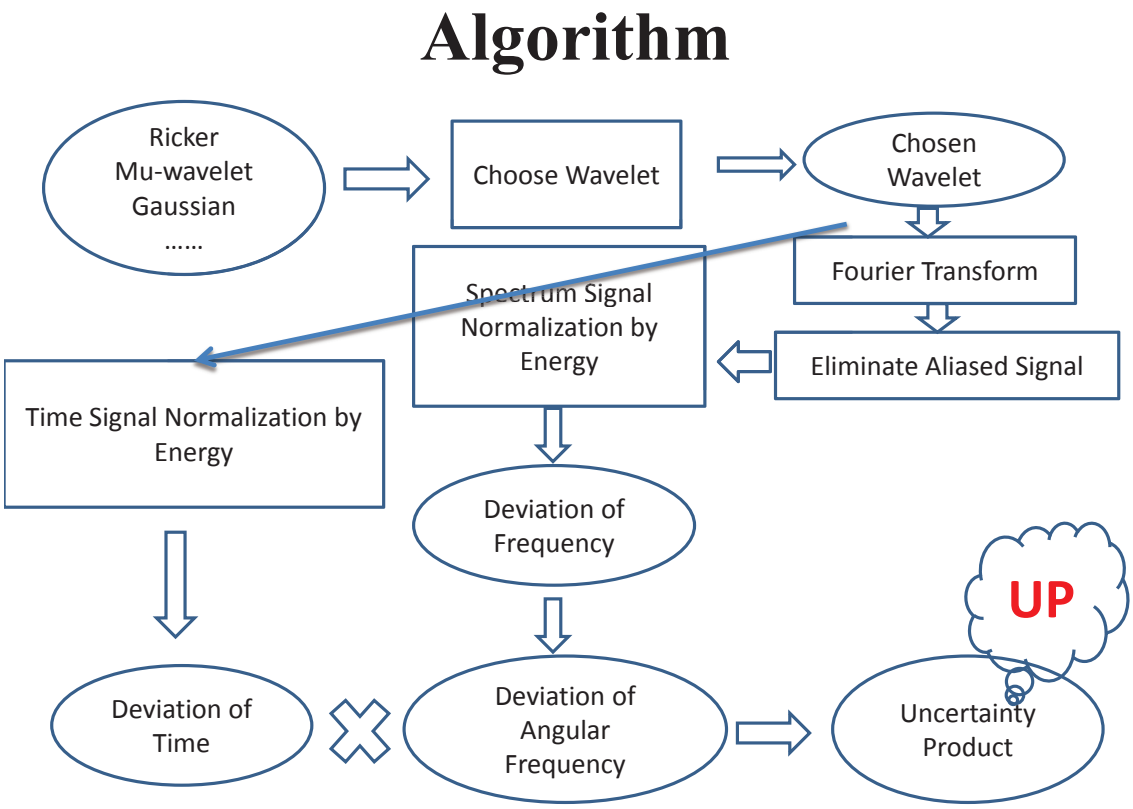

Figure 4.1: Procedures of calculating UP

4.6 Deeper Investigation of Uncertainty Product

Conventional UP can also be expressed as the width of the waveform in time times the bandwidth of the spectrum. However, we use the whole spectrum as shown in Figure 4.4a, containing both the positive and negative spectrum, in calculating the conventional UP, whose results are shown in Figure 4.3. The results are mathematically meaningful, but are they physically meaningful?

Negative frequency won't occur in reality, plus the spectrum we use in spectral decomposition is only the positive part, it seems meaningless to add negative frequency

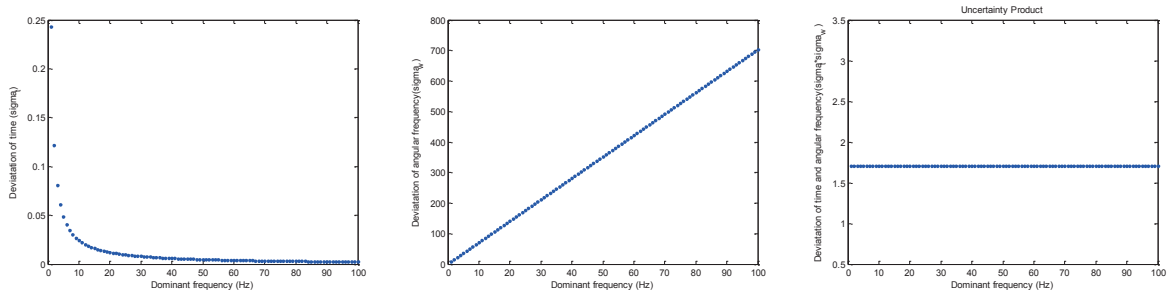

(a) σ_t of Ricker (b) σ_ω of Ricker (c) UP of Ricker

Figure 4.2: Results of standard deviation and UP of Ricker

into uncertainty product calculation. What we really care in spectral decomposition is only the positive spectrum. Since the negative part of the spectrum is the complex conjugate of the positive spectrum, we can easily reconstruct the negative spectrum from the positive spectrum. Due to the Hilbert transform, positive part of the spectrum means everything. Therefore, from a more practical point of view, we should adjust the way we calculate uncertainty product, ignore the negative part of spectrum. In my opinion, the reason why we have the negative frequency from Fourier transform is we have $cos(-wt)$ and $cos(wt)$ both orthogonal to $cos(wt)$ at the same time. Whereas, if we use complex representation of signal, we only have $exp(ix)$ orthogonal to $exp(-ix)$. Is the uncertainty principle still valid if we use complex representation of signal instead of real time signal? It seems so, those two assumptions of inequality in mathematical derivation of lowest limit won't change whether the signal is represented by complex time or real time.

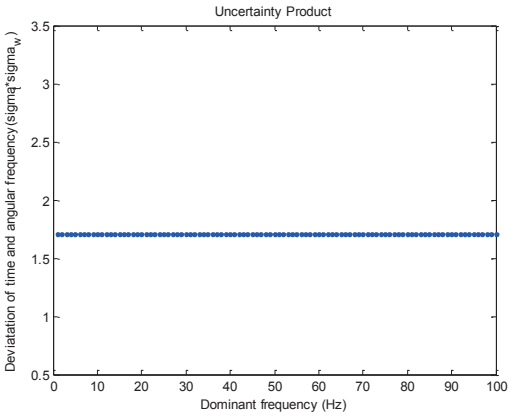

(a) UP of Ricker

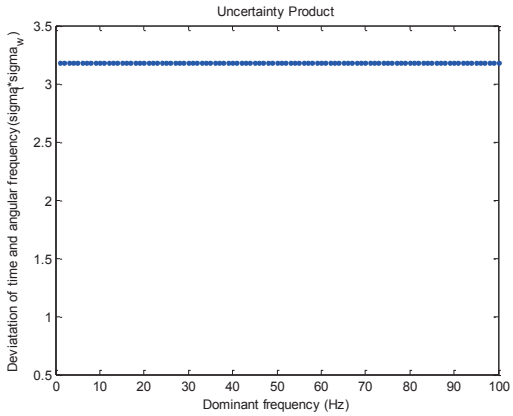

(b) UP of Morlet

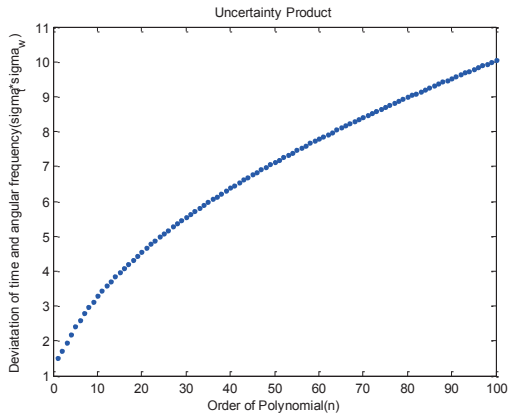

(c) UP of mu

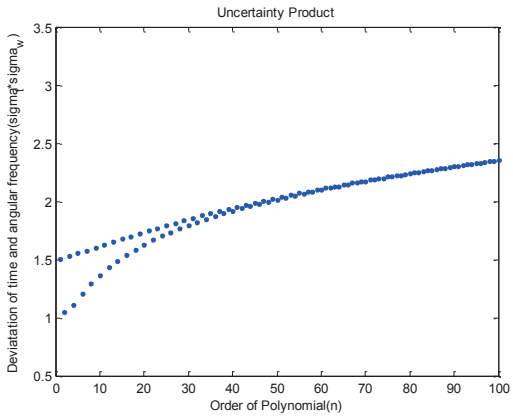

(d) UP of pseudo mu

Figure 4.3: Conventional UP of wavelets

4.7 Results of Complex Uncertainty Product

Therefore, if we calculate the uncertainty product using complex wavelets generated by Hilbert transform, Figure 4.5 is what we get which we call complex uncertainty product.

From the results showing above, the rule on lowest limit of uncertainty product breaks. We have lower limit than 1/2. By carefully examination, we discovered that

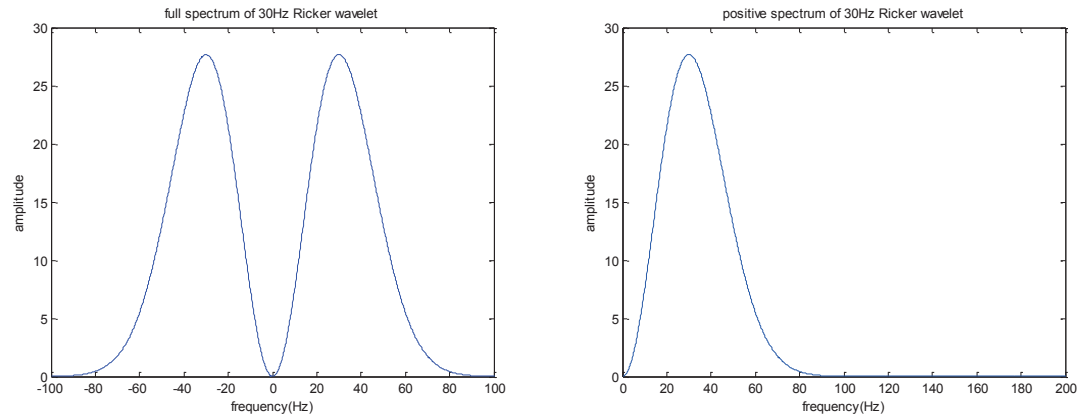

(a) Full spectrum of 30Hz Ricker

(b) Positive spectrum of 30Hz Ricker

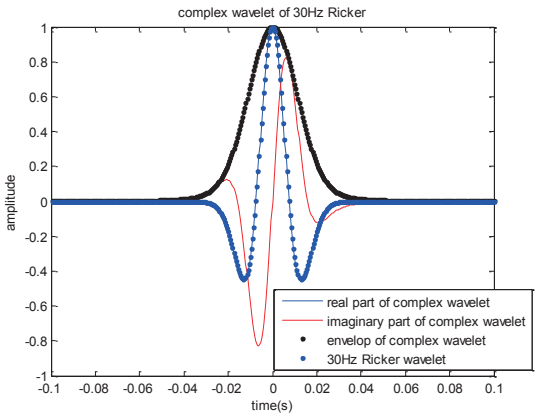

(c) Ricker in time

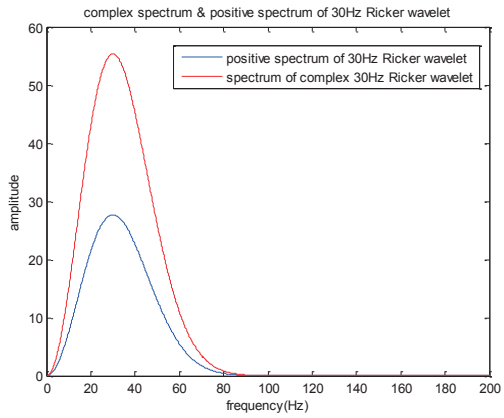

(d) Ricker in frequency

Figure 4.4: Comparison between conventional UP and complex UP

those wavelets which have uncertainty product of lower than 1/2 all have one thing in common. They violate zero mean condition in choosing wavelets.

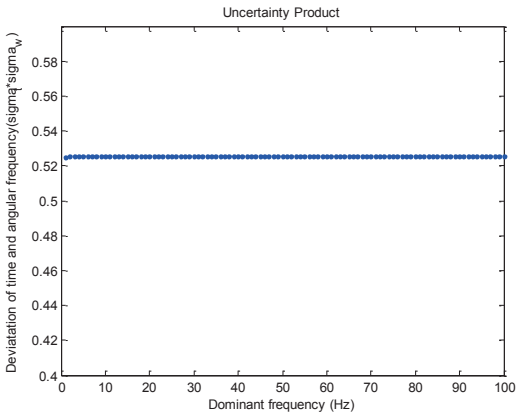

(a) UP of Ricker

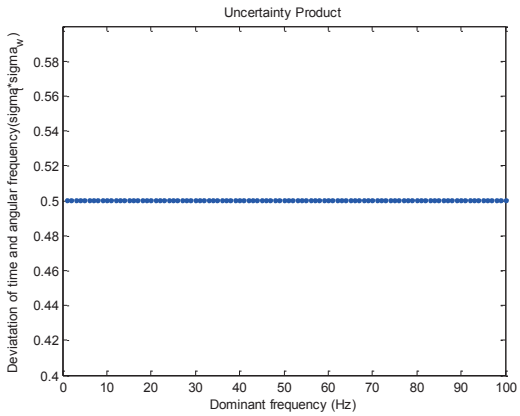

(b) UP of Morlet

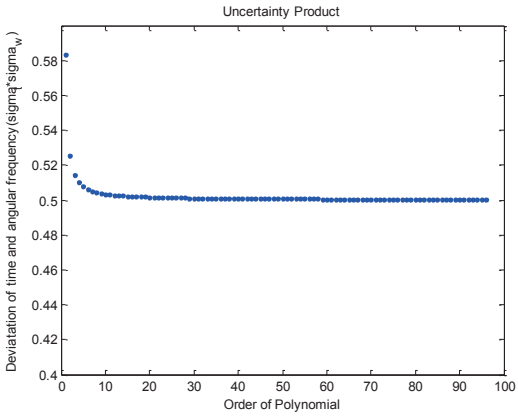

(c) UP of mu

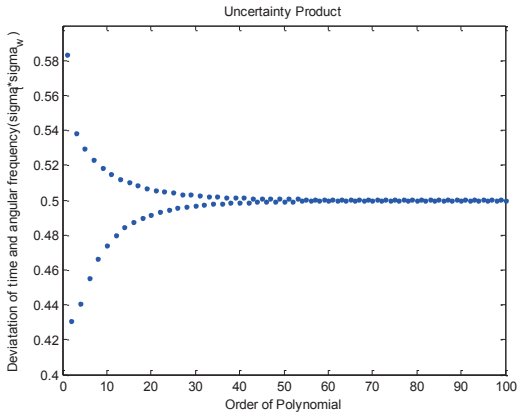

(d) UP of pseudo mu

Figure 4.5: Complex UP of wavelets

Chapter 5

Thickness Estimation

5.1 Need for Accurate Thickness Estimation

You won't hesitate to drill a well if your reservoir is enormously large. However, when you are dealing with unconventional reservoir or small reservoir, you need to evaluate, take a deeper thought on whether to drill or not, whether this well is worth drilling, or should we skip it. By estimating the whole volume, porosity, and recovery factor of the reservoir, we know the economic value of this reservoir. Based on that information, we decide to drill a well or not. Thickness estimation is the key in calculating the volume of the reservoir. Therefore, how to estimate the thickness? Which method is more accurate?

5.2 Resolution Limit

Seismic responses are the results of convolution of wavelets and reflectivity. Based on just the amplitude map, we suffered from resolution problem, which means we can hardly resolve extreme thin layers. Even though we can detect there is a thin bed over there, we can hardly tell the top and base of the thin bed just simply base on the amplitude map. "Resolvability" is the ability to separate two events. "Detectability" is the ability to know the existence of the events. Therefore, the question remains what is the resolution limit of seismic data?

5.3 Resolution Criterion

There are three major kinds of resolution criteria, which are fully discussed by Kallweit and Wood1982, and I paraphrase as followed:

5.3.1 Rayleigh's Criterion

Two wavelets are resolved when their separation are larger than or equal the time interval from peak to trough of the convolving wavelet.

5.3.2 Ricker's Criterion

Two wavelets are resolved when their separation are larger or equal than the time interval between two inflection points in the primary lobe of the convolving wavelet. When the time separation between two wavelets is below the interval of two inflection points of the convolving wavelet, the shape of the waveform becomes like one larger

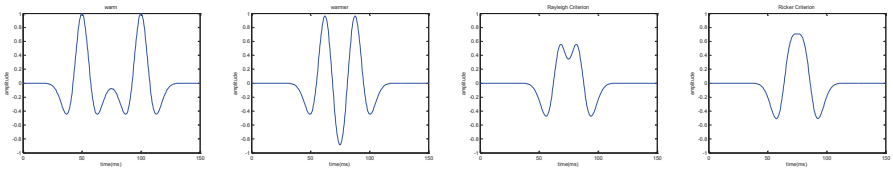

(a) start to interfere (b) closer (c) Rayleigh's (d) Ricker's

Figure 5.1: Resolution illustration of Rayleigh criterion and Ricker criterion

event. There comes no depression between those two wavelets, instead, we see a clear flat top.

5.3.3 Widess's Criterion

While Rayleigh and Ricker considered two positive reflections, Widess considered two opposite reflections. Widess discovered that when two wavelets are closer than a quarter of the predominant period of the incident wavelet, the shape of the waveform approaches the time derivative of the incident wavelet. There Widess defined a quarter of the predominant period of the incident wavelet as the highest limit of a thin bed. The derivative of a wavelet looks like the wavelet with a 90 degree phase shift. Therefore, base on the waveform, we cannot tell whether the waveform is result of one event or two, in other words, we cannot resolve this thin bed.

5.3.4 Tuning Thickness

Widess said that [Widess, 1973], it is appropriate to define a thin bed as one whose actual thickness is below one eighth of the predominant wavelength, whose time thickness is below one quarter of the predominant period, based on the reason that, the derivative of the convolving wavelet times a constant factor looks similar to two

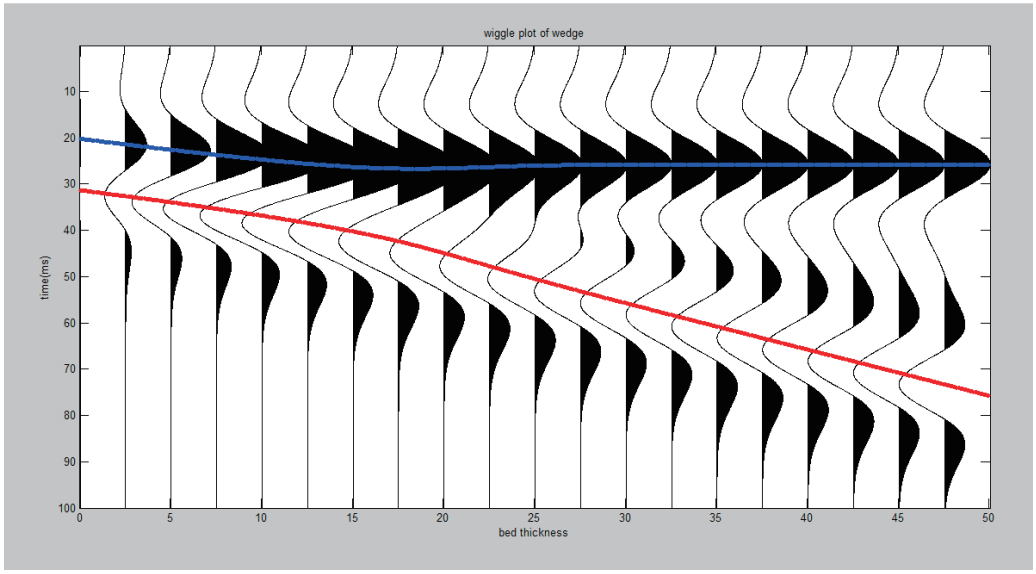

Figure 5.2: Wiggle plot of wedge model

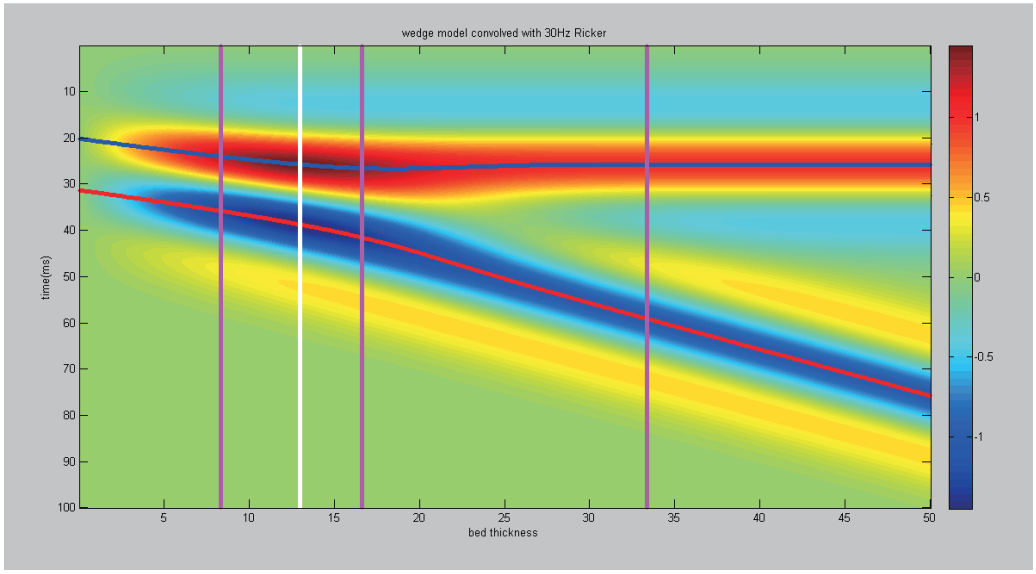

Figure 5.3: Peak and trough of wedge model

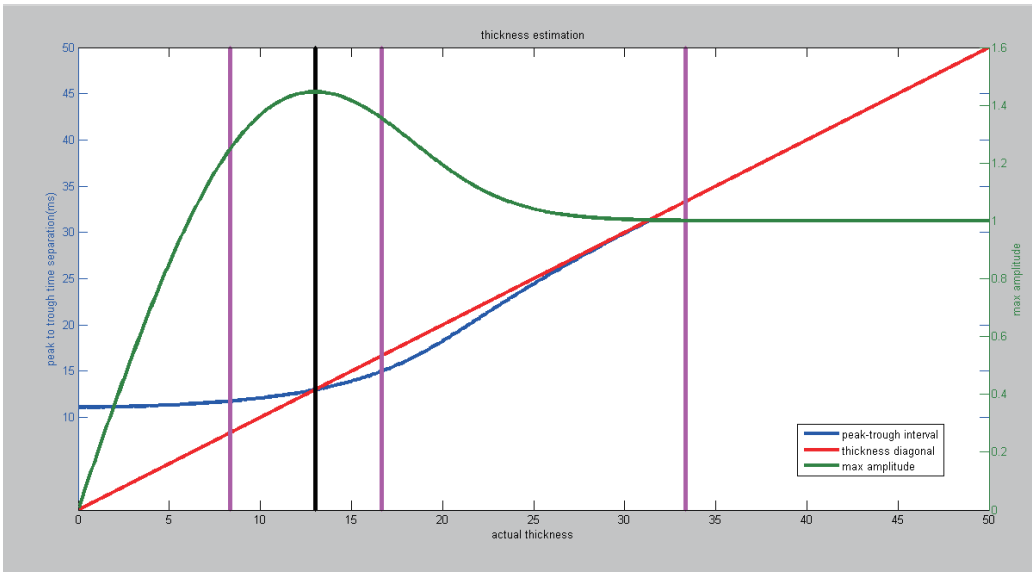

Figure 5.4: Thickness estimation: amplitude method

wavelets convolving with a thin bed whose reflection coefficients are opposite equal value as shown in Figure 5.5. It is reasonable to deduce that the tuning thickness is whose time thickness equals one quarter of the predominant period. However, when we take a look at the max amplitude of the reflection as shown in Figure 5.4, the big change of the amplitude is not exactly located at one quarter of the predominant period. Someone may want to define tuning thickness exactly at where the max amplitude of the trace starts to decrease which is more reasonable from my point of view. In that case, the tuning thickness is exactly the Rayleigh's criterion, peak to trough interval. The peak to trough interval of Ricker wavelet was derived by Chung and Lawton [1995] which can be calculated in Eq. 5.1.

$$t_{p-t} = \frac{\sqrt{6}}{2\pi f_{dom}} \tag{5.1}$$

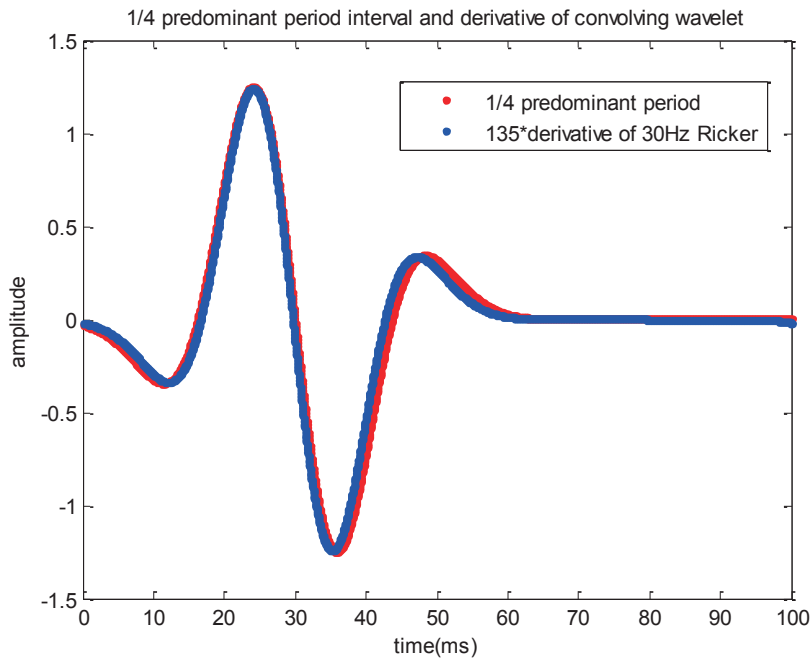

Figure 5.5: 1/4 predominant period of separation versus derivative of convolving wavelet

The tuning thickness I refer to is always relating to Rayleigh's criterion from now on.

5.3.5 Below Tuning

5.3.5.1 Amplitude Method

From Figure 5.4, we can see that below tuning thickness, the amplitude decrease with the decrease of bed thickness, and the trend is almost linear. So Widess suggests that we can use this linear relationship to estimate the thickness of thin beds.

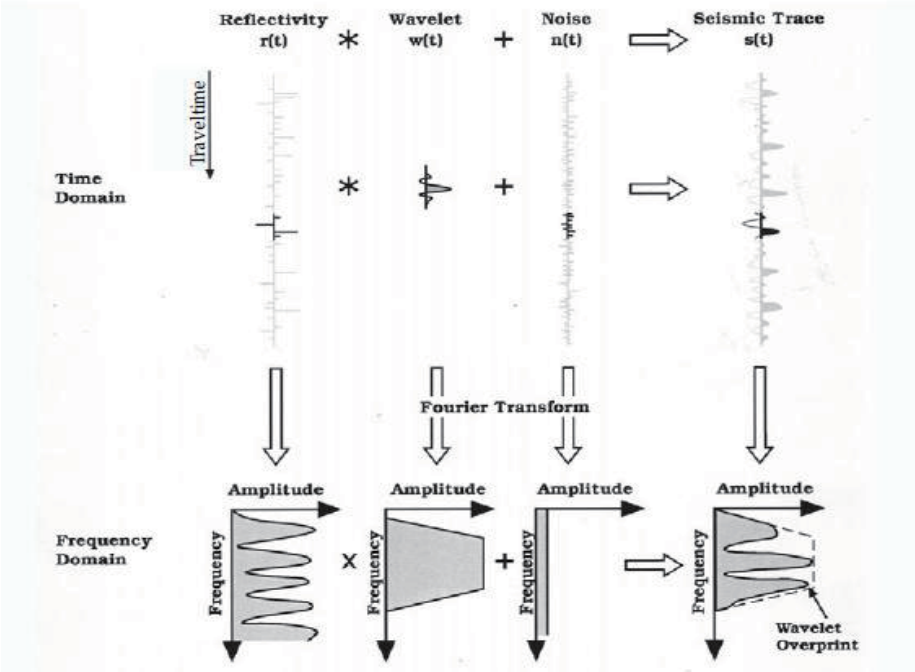

Figure 5.6: Illustration of relationship between bed thickness and periodic notches in frequency [Partyka et al., 1999]

5.3.5.2 Spectral Method

Frequency representation is analogous to time representation of a signal. From frequency, we can extract coded information of time properties. Partyka [Partyka et al., 1999] had discovered one which revealed the relationship between bed thickness and periodic notches in frequency as shown in Figure 5.6.

Partyka had compared these methods in his paper [Partyka, 2001], he had discussed the pros and cons of different methods in thickness estimation. However, in my point of view, spectral method is left to be further explored. I believe, in the future research, spectral method would show promising results in thickness estimation.

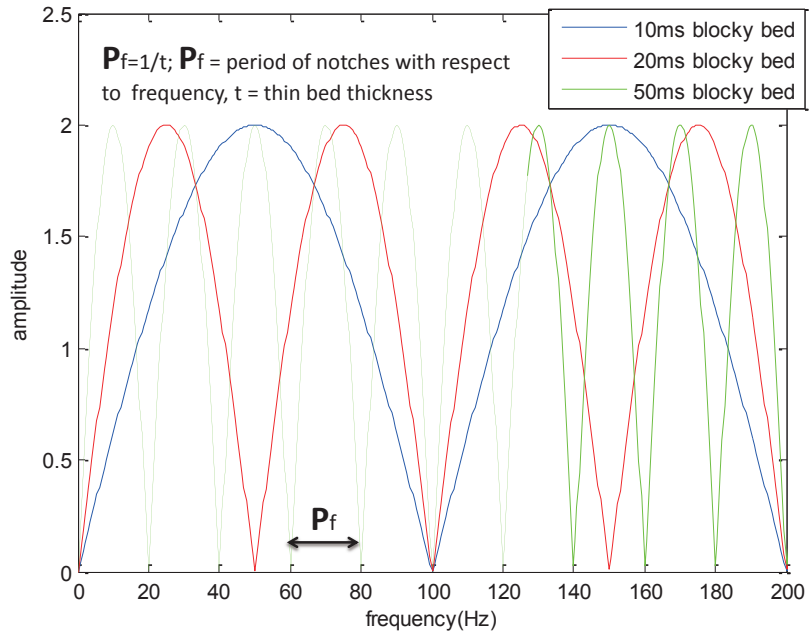

Figure 5.7: Thickness slice of spectral amplitude modified from [Partyka et al., 1999]

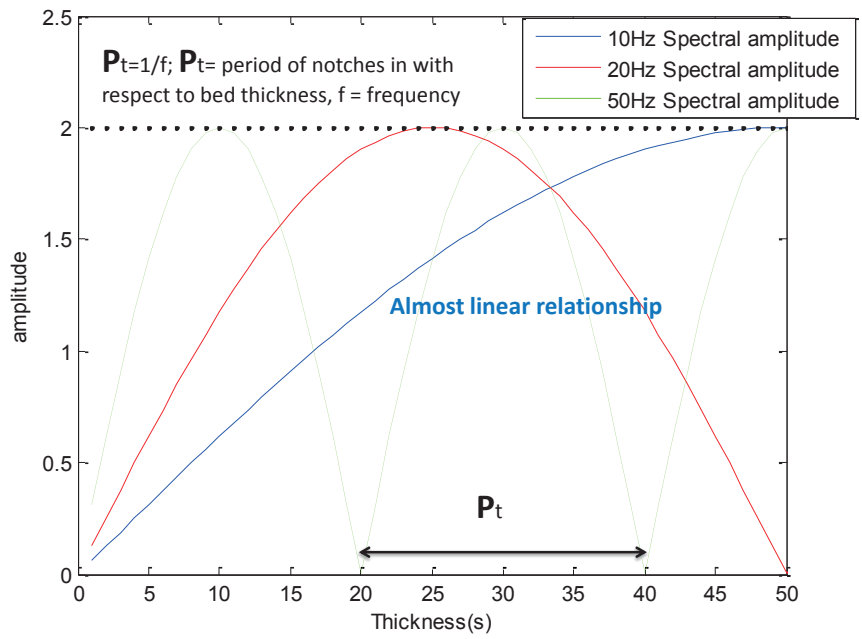

Figure 5.8: Frequency slice of spectral amplitude modified from [Partyka et al., 1999]

Appendix A

Comparison Results of MPD and FMPD on Dickman Dataset: Vertical Section

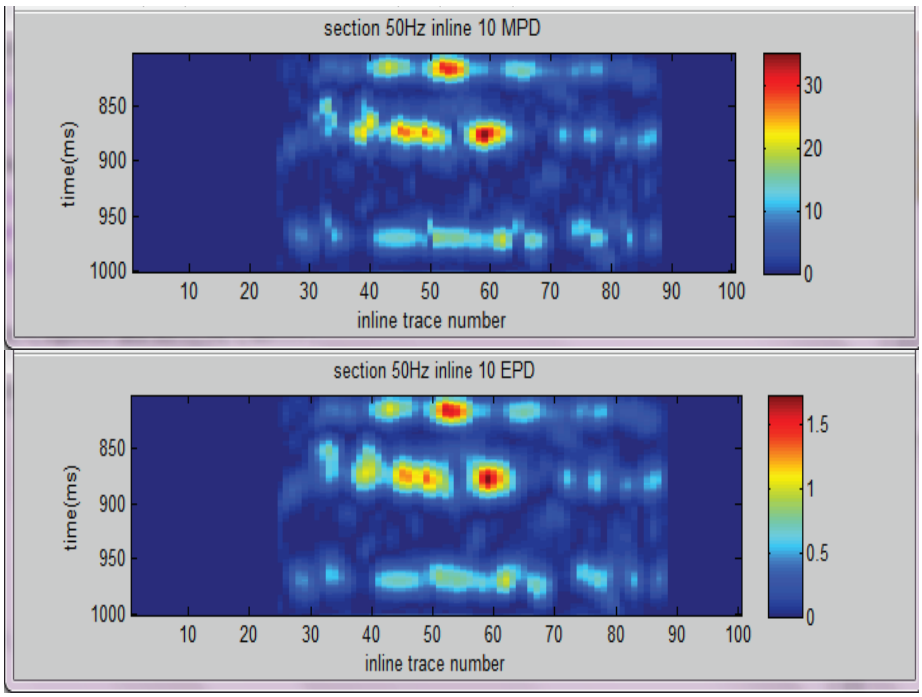

Figure A.1: MPD and FMPD results of vertical section inline 10 at 50Hz

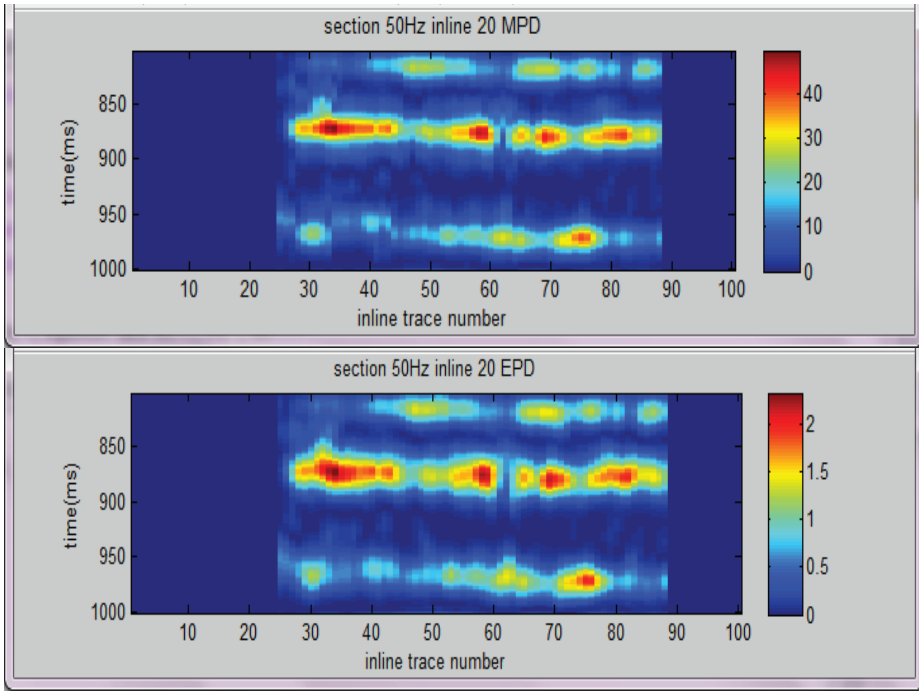

Figure A.2: MPD and FMPD results of vertical section inline 20 at 50Hz

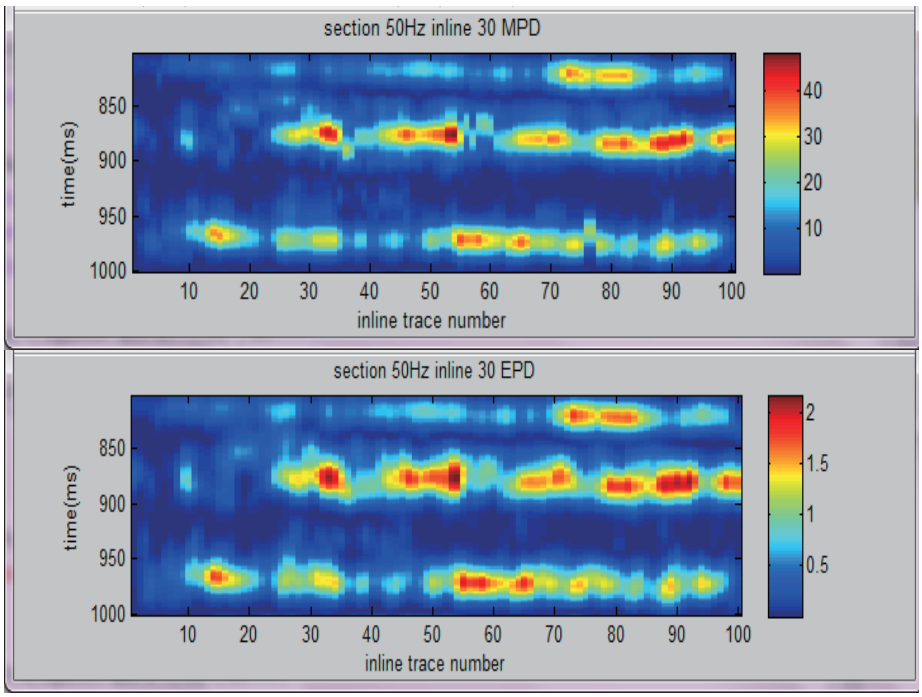

Figure A.3: MPD and FMPD results of vertical section inline 30 at 50Hz

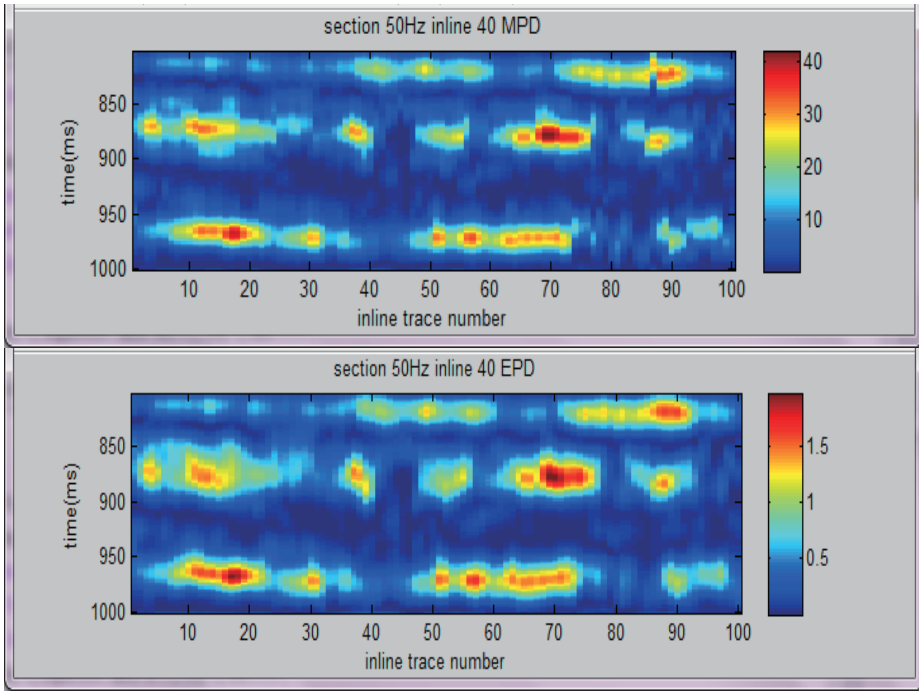

Figure A.4: MPD and FMPD results of vertical section inline 40 at 50Hz

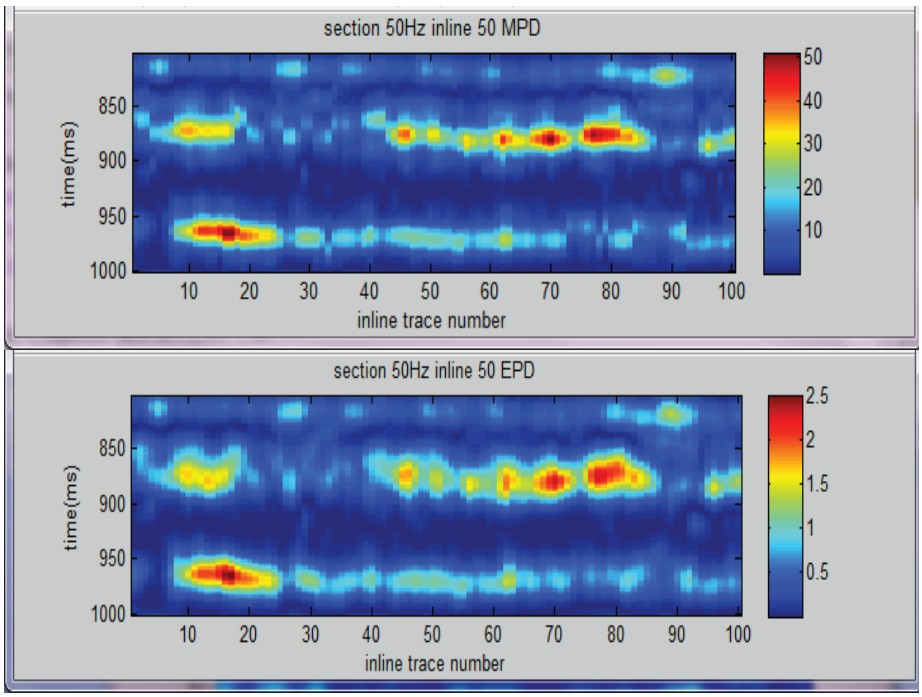

Figure A.5: MPD and FMPD results of vertical section inline 50 at 50Hz

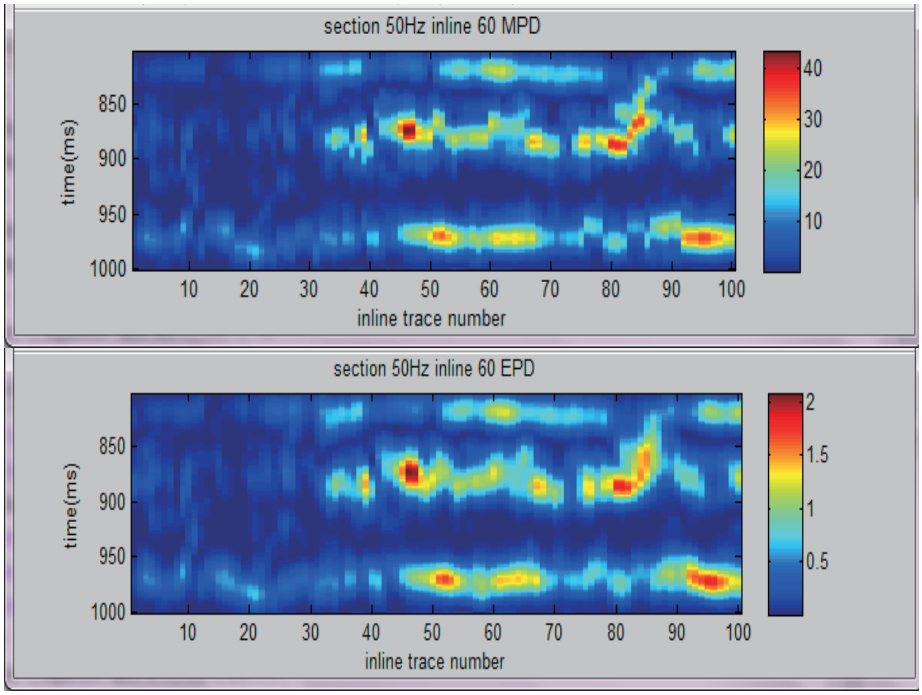

Figure A.6: MPD and FMPD results of vertical section inline 60 at 50Hz

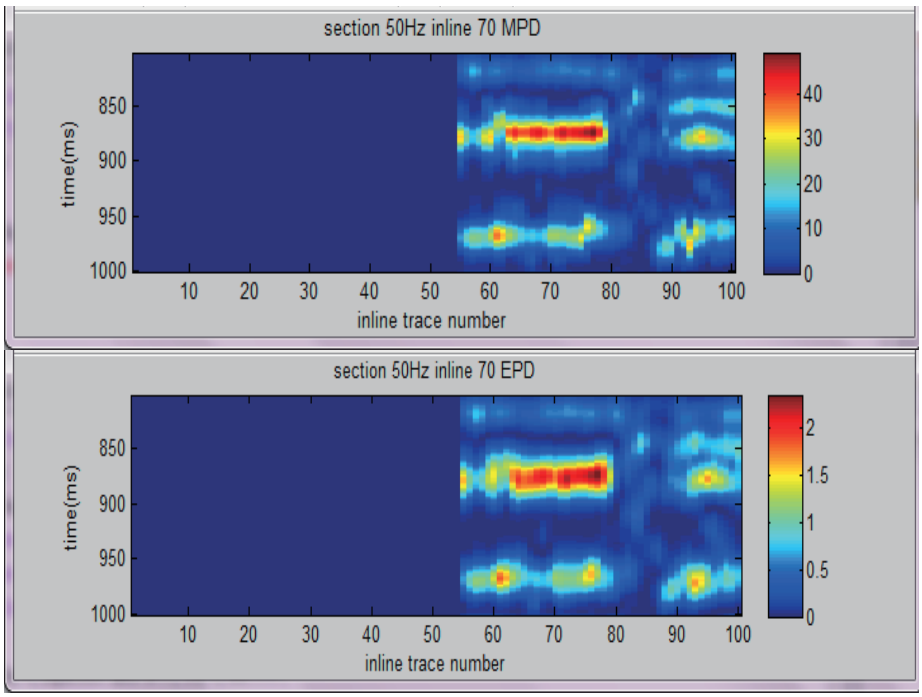

Figure A.7: MPD and FMPD results of vertical section inline 70 at 50Hz

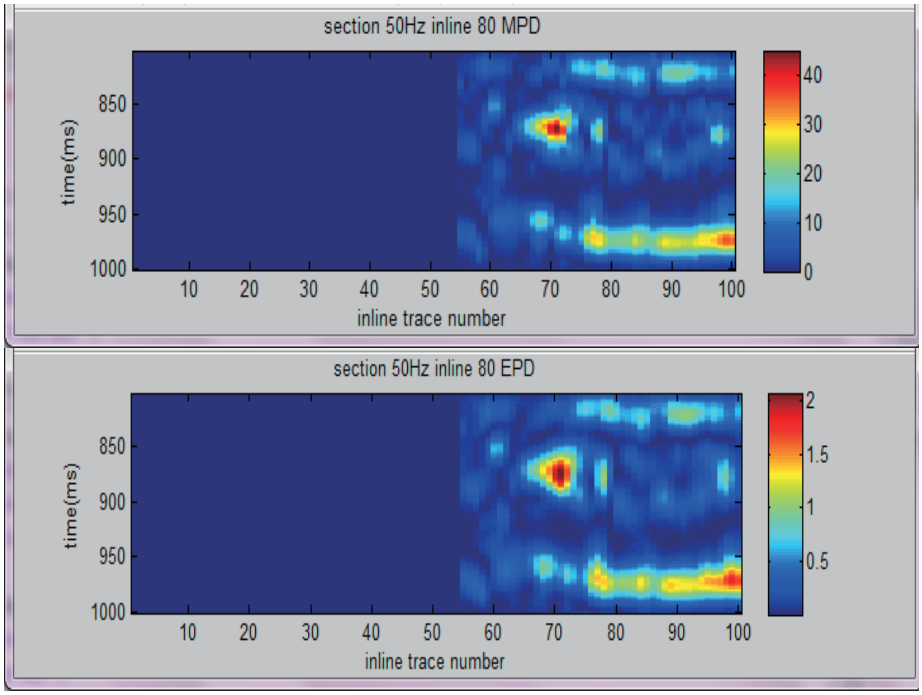

Figure A.8: MPD and FMPD results of vertical section inline 80 at 50Hz

Appendix B

Comparison Results of MPD and FMPD on Dickman Dataset: Time Slice

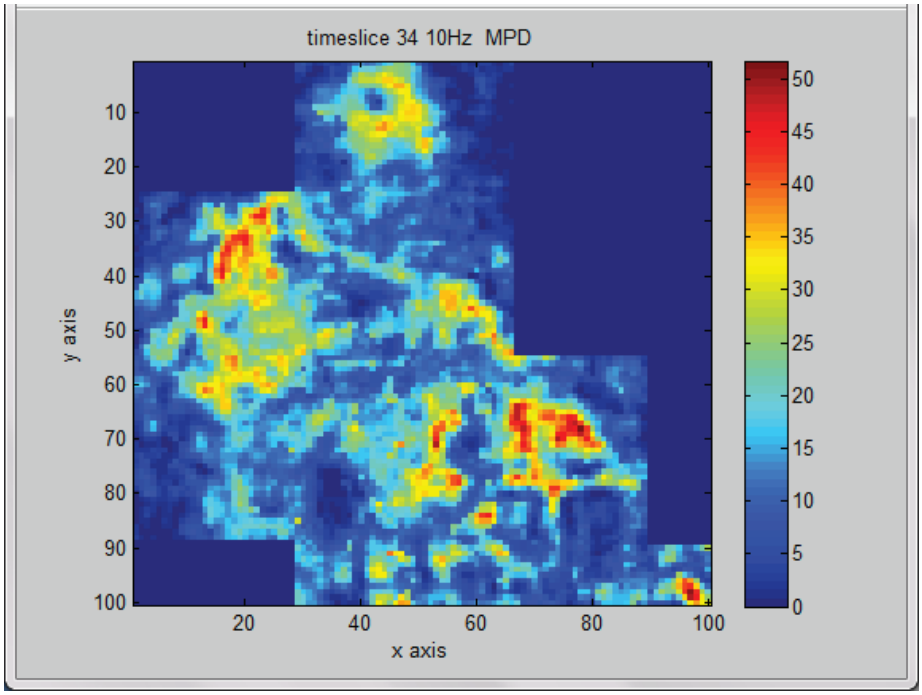

(a) MPD result

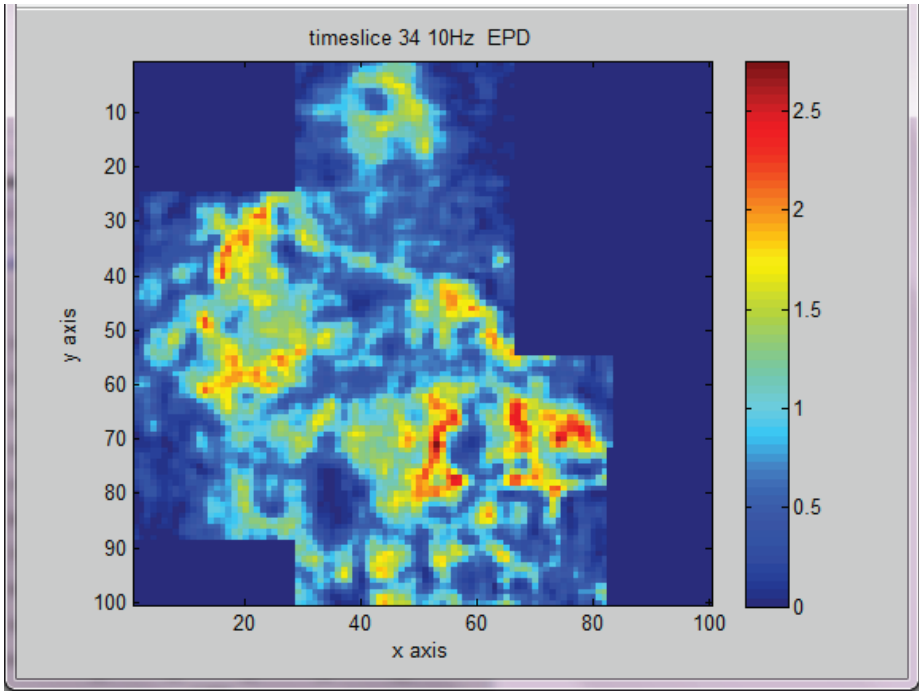

(b) FMPD result

Figure B.1: MPD and FMPD results of timeslice 868ms at 50Hz

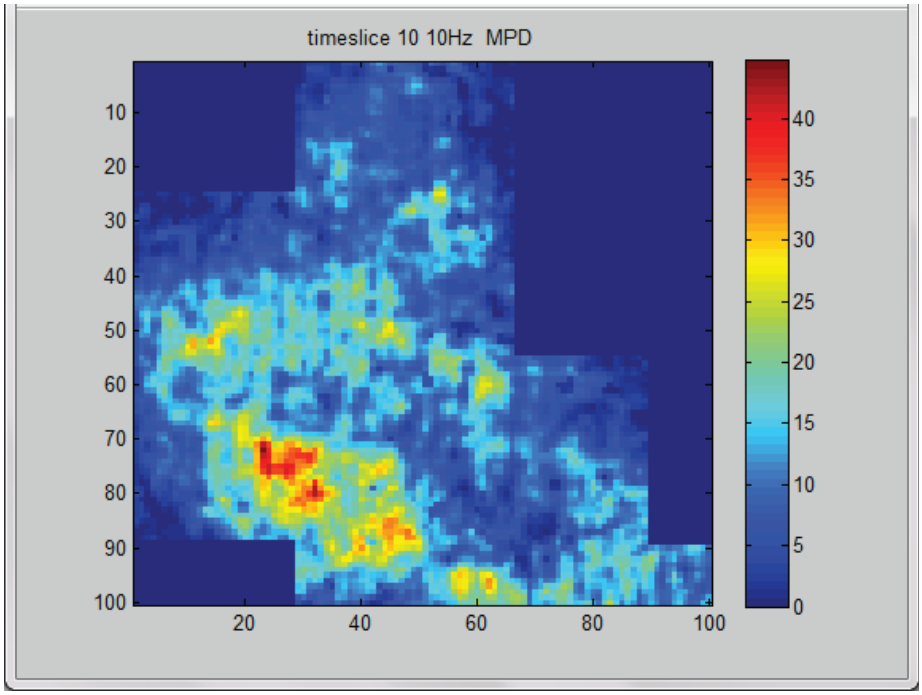

(a) MPD result

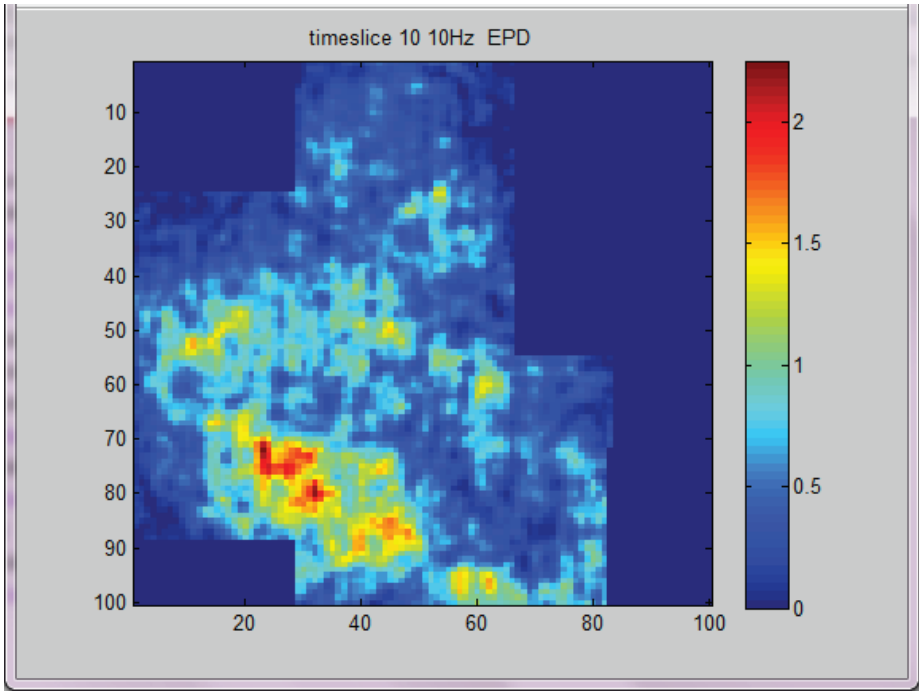

(b) FMPD result

Figure B.2: MPD and FMPD results of timeslice 820ms at 50Hz

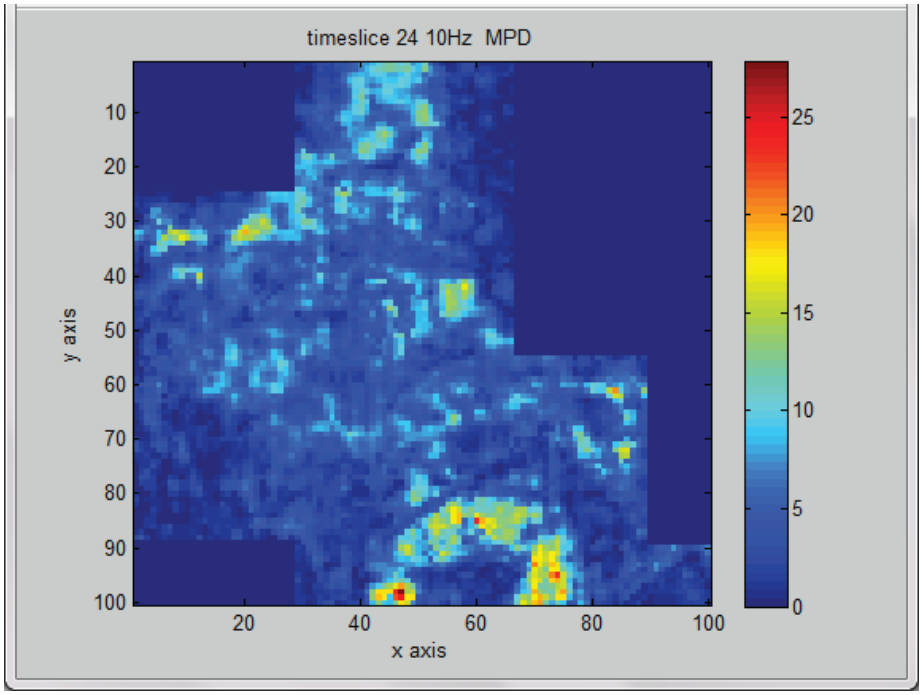

(a) MPD result

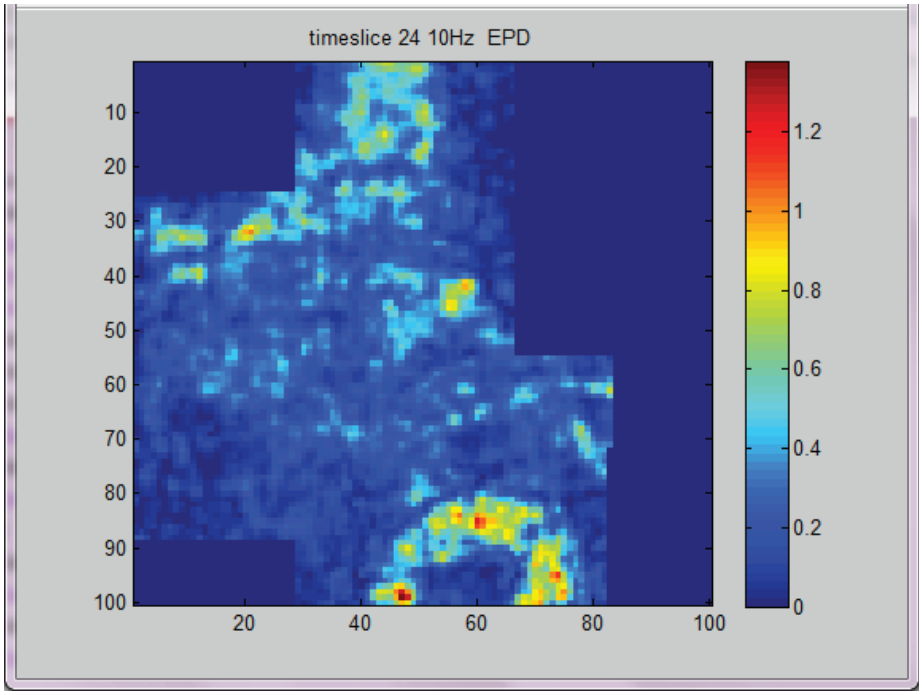

(b) FMPD result

Figure B.3: MPD and FMPD results of timeslice 848ms at 50Hz

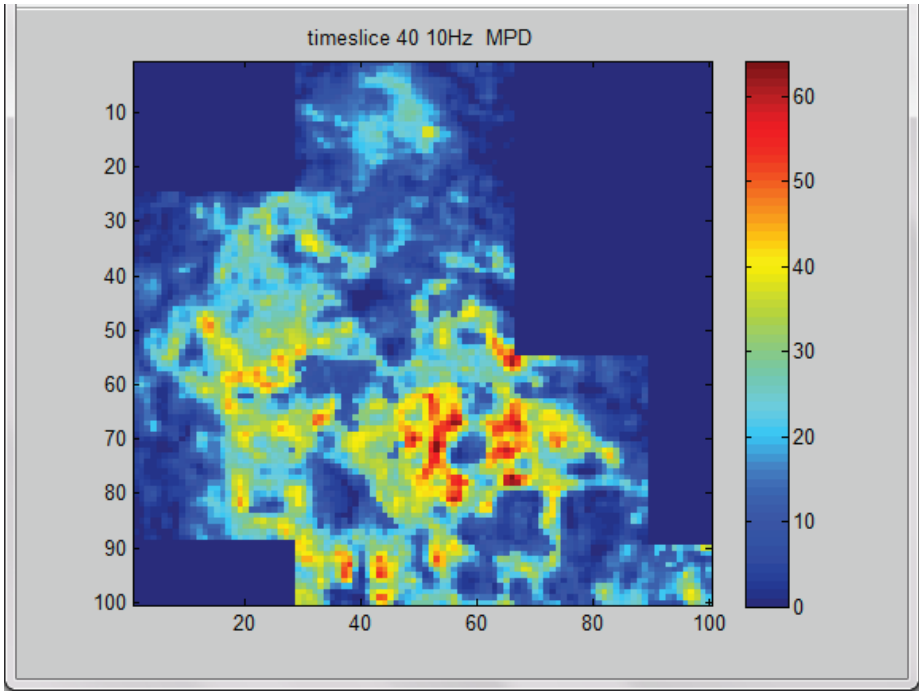

(a) MPD result

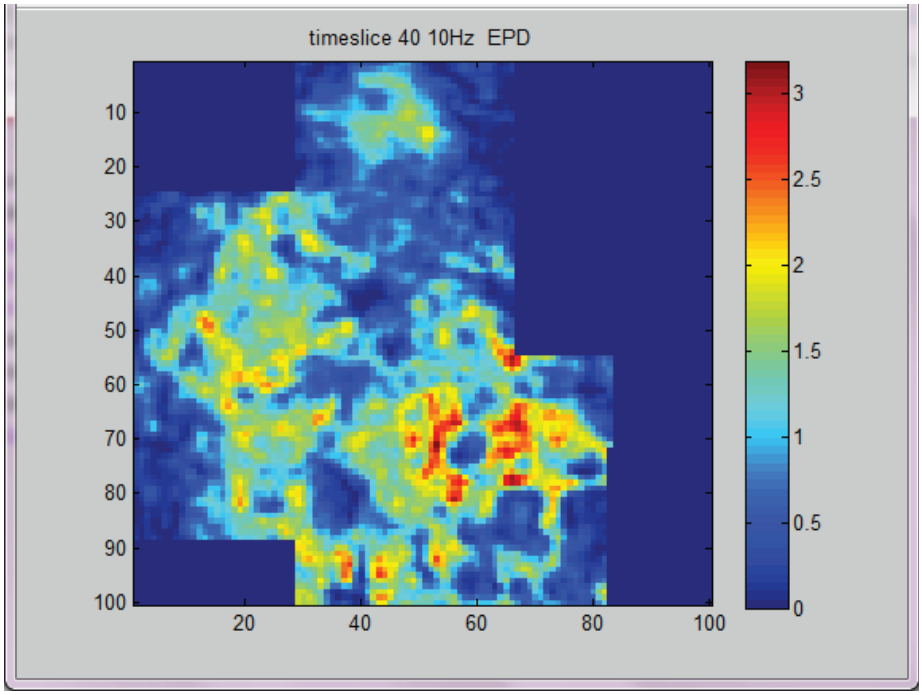

(b) FMPD result

Figure B.4: MPD and FMPD results of timeslice 880ms at 50Hz

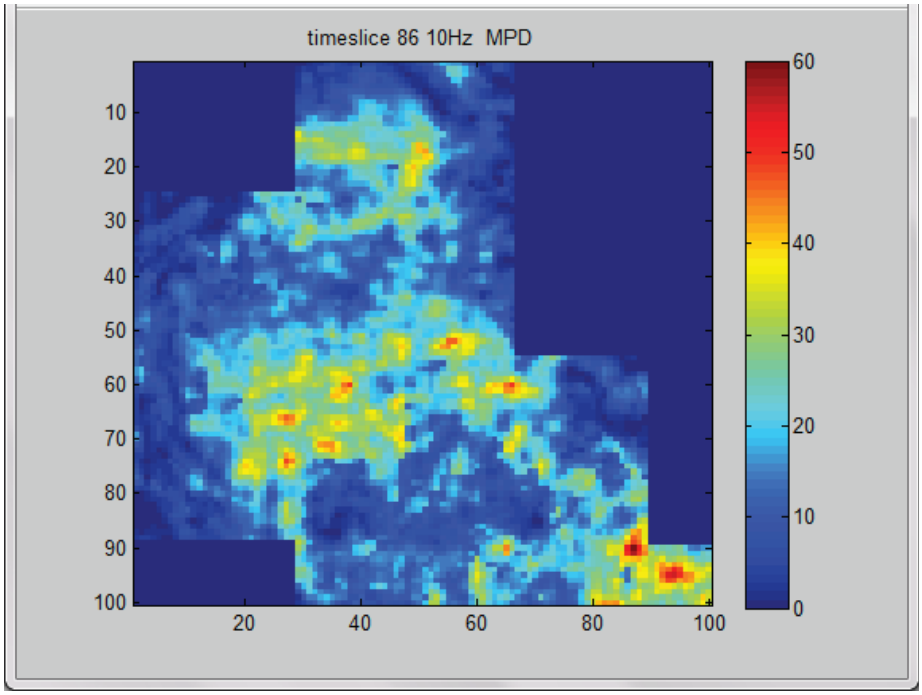

(a) MPD result

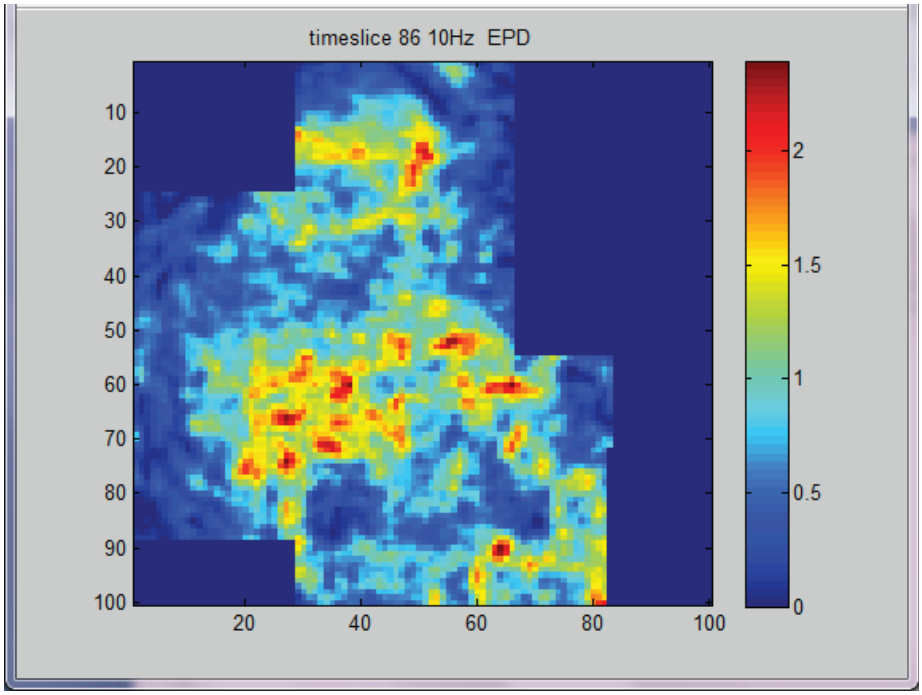

(b) FMPD result

Figure B.5: MPD and FMPD results of timeslice 972ms at 50Hz

Appendix C

Mathematical Definitions and Illustrations of Wavelets

C.1 Ricker wavelet

Formula:

$$S(t) = (1 - 2\pi^2 f^2 t^2) e^{-\pi^2 f^2 t^2} \tag{C.1}$$

C.2 Morlet wavelet

Formula:

$$S(t) = a_0 e^{-\beta^2 t^2} \cos(\omega_0 t + \varphi_0) \tag{C.2}$$

where in my application,

$$\beta = f;\ \omega_0 = 2\pi f;\ a = 1;\ \varphi_0 = 0$$

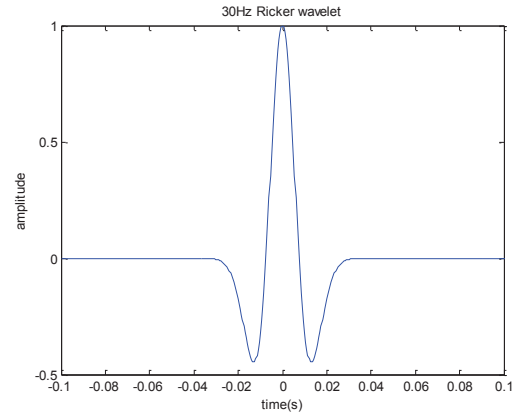

(a) Ricker waveform

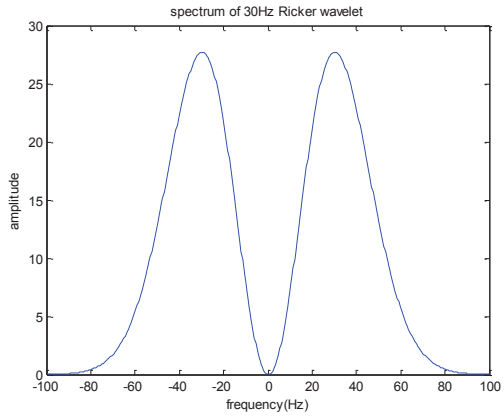

(b) Ricker spectrum

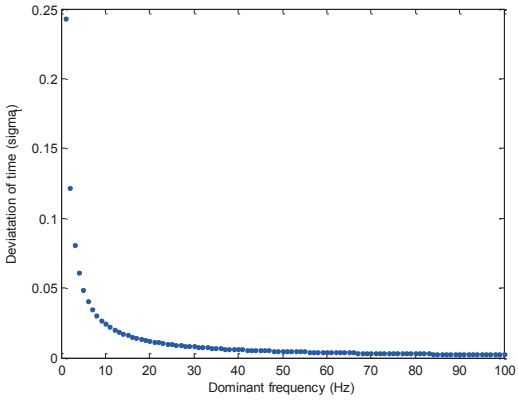

(c) Conventional σ_t of Ricker

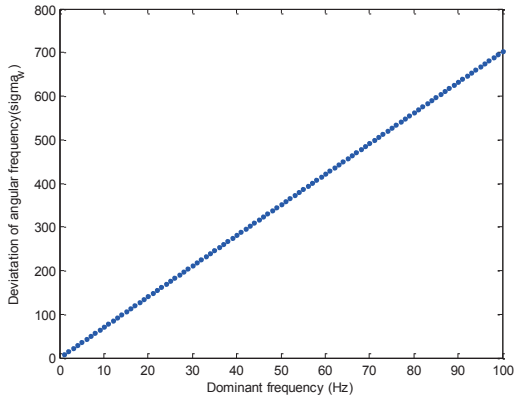

(d) Conventional σ_ω of Ricker

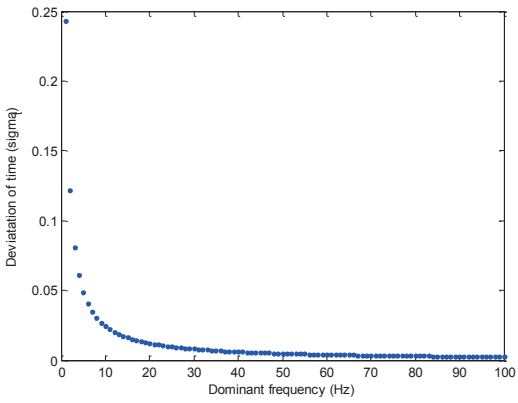

(e) Complex σ_t of Ricker

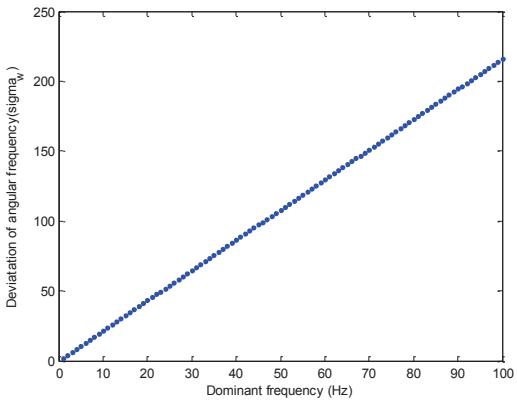

(f) Complex σ_ω of Ricker

Figure C.1: Illustration of Ricker wavelets

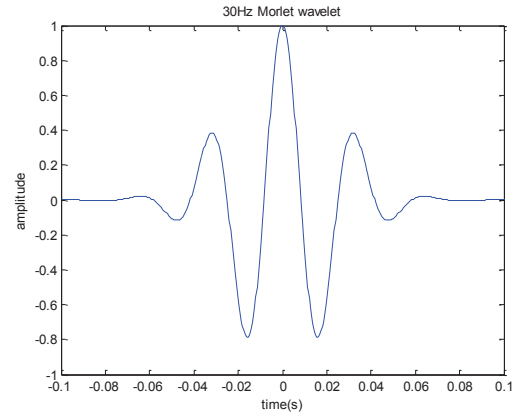

(a) Morlet waveform

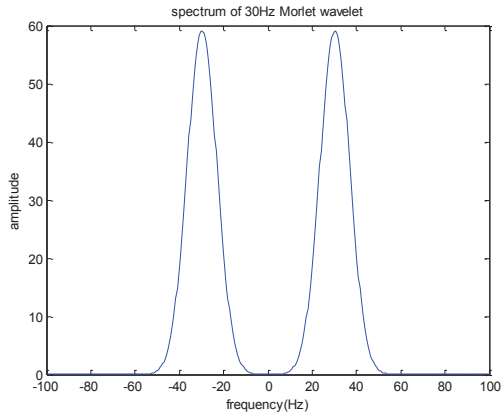

(b) Morlet spectrum

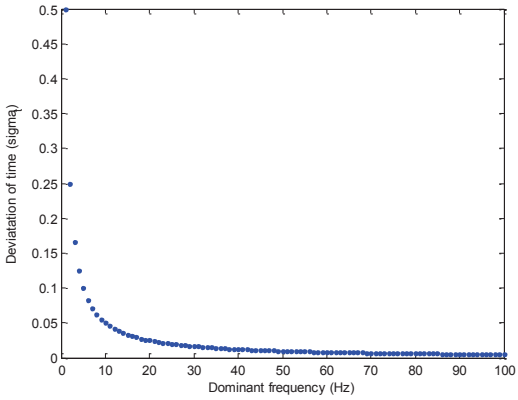

(c) Conventional σ_t of Morlet

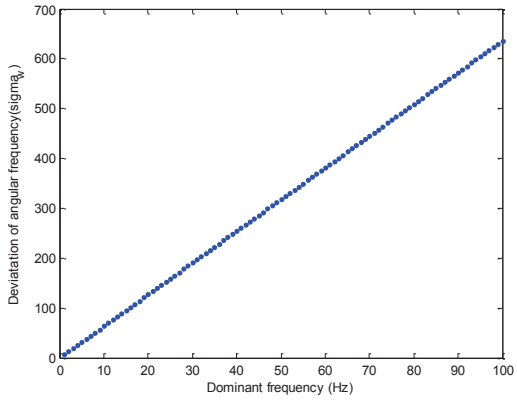

(d) Conventional σ_ω of Morlet

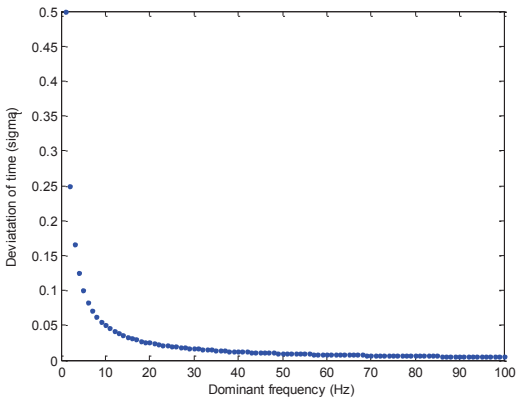

(e) Complex σ_t of Morlet

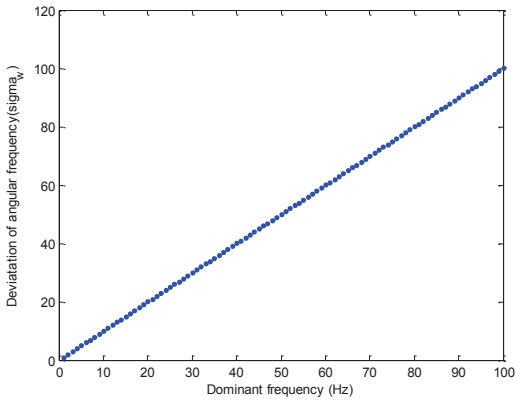

(f) Complex σ_ω of Morlet

Figure C.2: Illustration of Morlet wavelets

C.3 μ and pseudo μ wavelets

Formula: μ and pseudo μ wavelets are generated from Hermite polynomials. Hermite Polynomials:

$$H_n(t) = (-1)^n e^{t^2} \frac{d^n}{dt^n} e^{-t^2} \tag{C.3}$$

It is easier to code using the following recursion formula,

$$\begin{cases} H_{n+1}(t) = 2tH_n(t) - 2nH_{n-1}(t) \\ \\ H_0(t) = 1 \ and \ H_1(t) = 2t \end{cases} \tag{C.4}$$

Then, we have μ wavelets,

$$\mu_n^{\lambda,\sigma}(t) = N_n H_n(x) e^{-x^2} \tag{C.5}$$

And pseudo μ wavelets,

$$\mu_n^{\lambda,\sigma}(t) = N_n H_n(x) e^{-x^2\sqrt{n}} \tag{C.6}$$

where,

$$x = \frac{\sqrt{\lambda}(t-\tau)}{\sigma} \quad \& \quad N_n = \frac{1}{\sigma(\sqrt{2n \star n! \sqrt{n}})}$$

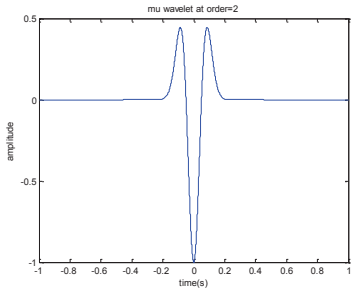

(a) μ waveform order=2

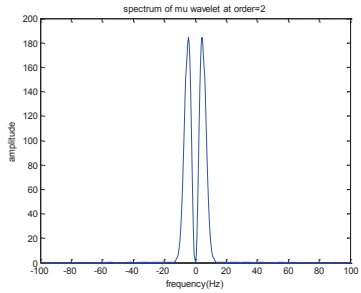

(b) μ spectrum order=2

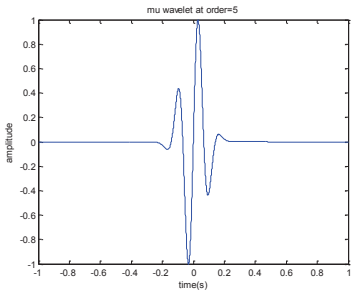

(c) μ waveform order=5

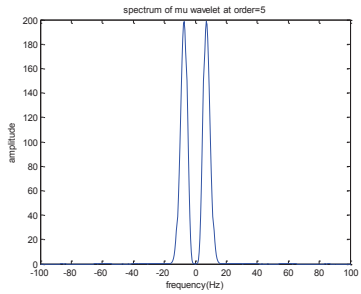

(d) μ spectrum order=5

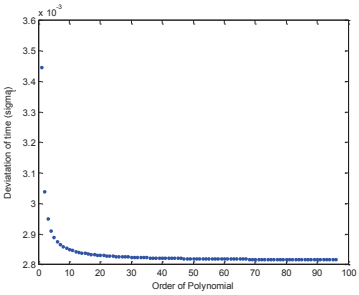

(e) Conventional σ_t of μ

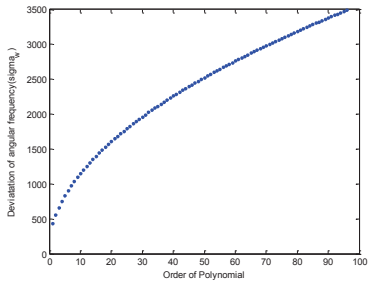

(f) Conventional σ_ω of μ

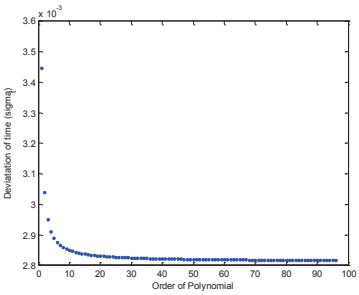

(g) Complex σ_t of μ

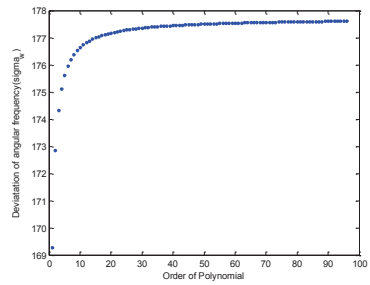

(h) Complex σ_ω of μ

Figure C.3: Illustration of μ wavelets

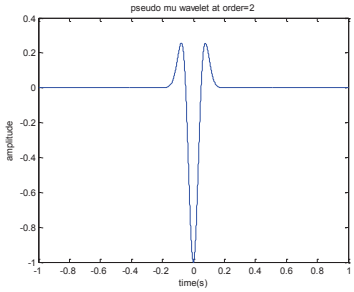

(a) pseudo μ waveform order=2

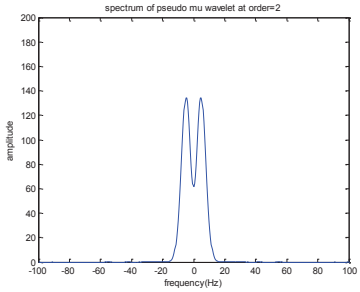

(b) pseudo μ spectrum order=2

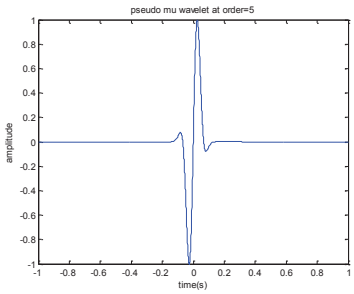

(c) pseudo μ waveform order=5

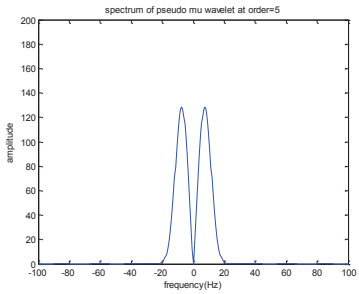

(d) pseudo μ spectrum order=5

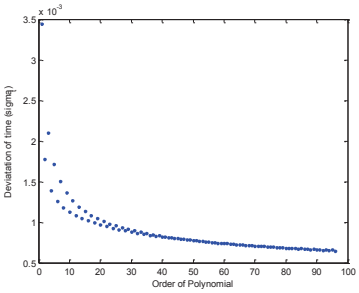

(e) Conventional σ_t of pseudo μ

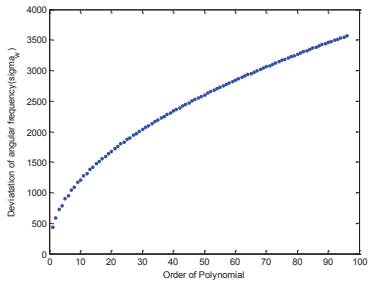

(f) Conventional σ_ω of pseudo mu

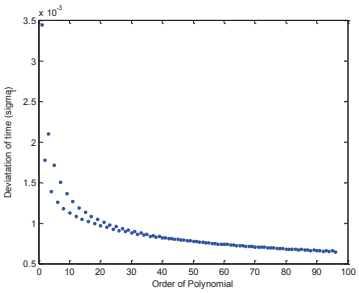

(g) Complex σ_t of pseudo μ

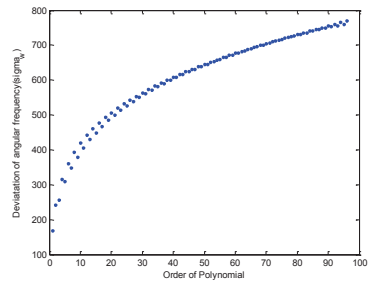

(h) Complex σ_ω of pseudo μ

Figure C.4: Illustration of pseudo μ wavelets

Appendix D

Various Wavelets in Temporal and Spectral Domain

D.1 Ricker wavelets

D.2 Morlet wavelets

D.3 μ wavelets and pseudo μ wavelets

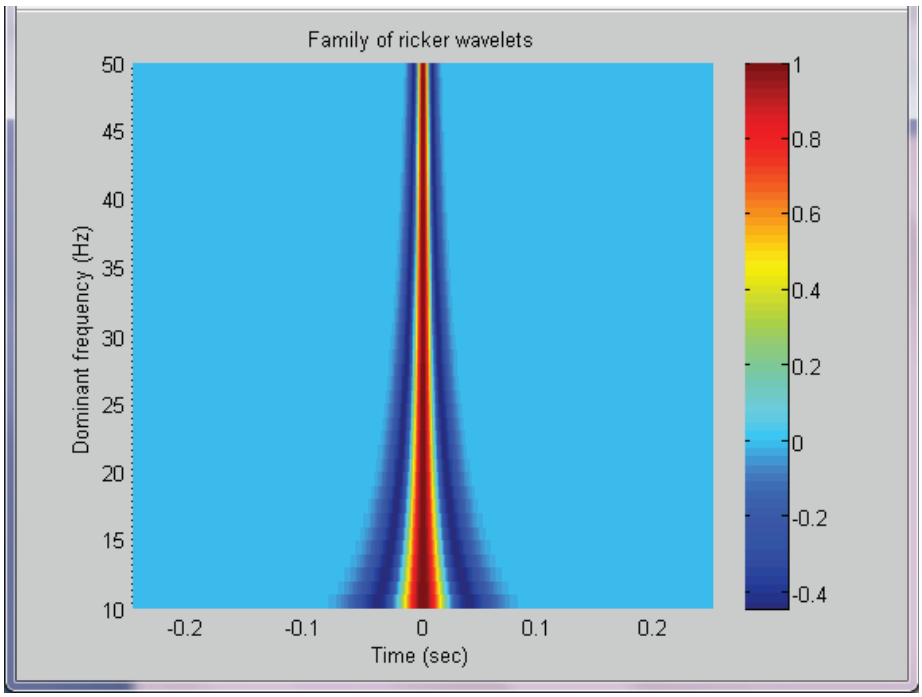

Figure D.1: Ricker wavelets in time

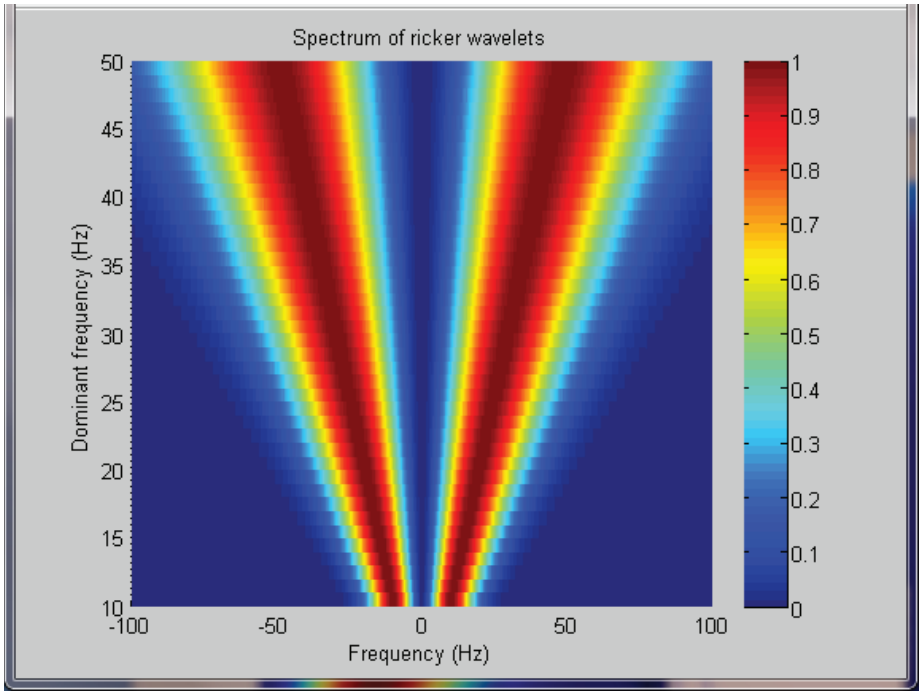

Figure D.2: Ricker wavelets in frequency

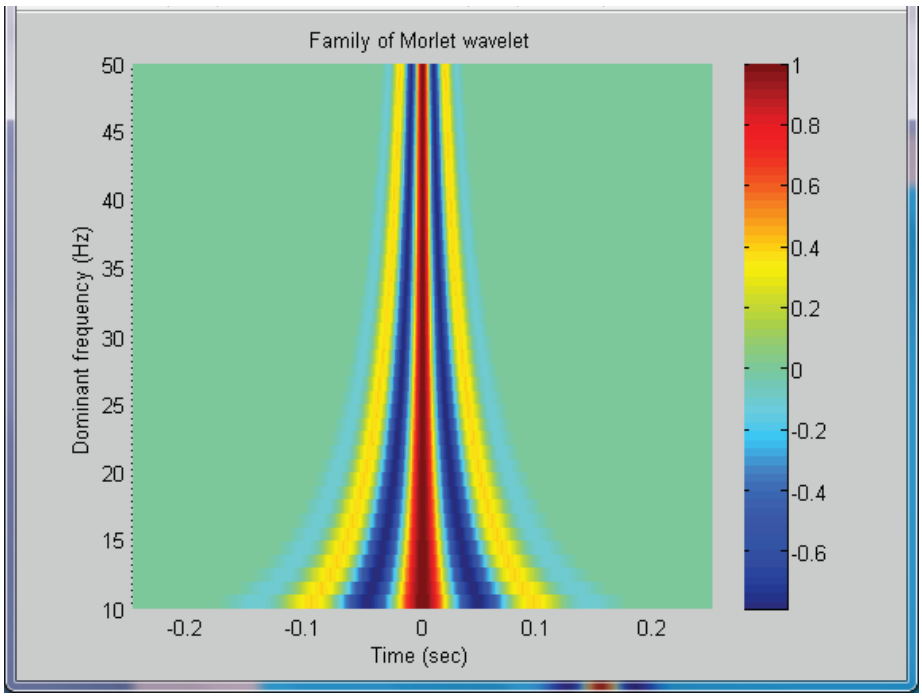

Figure D.3: Morlet wavelets in time

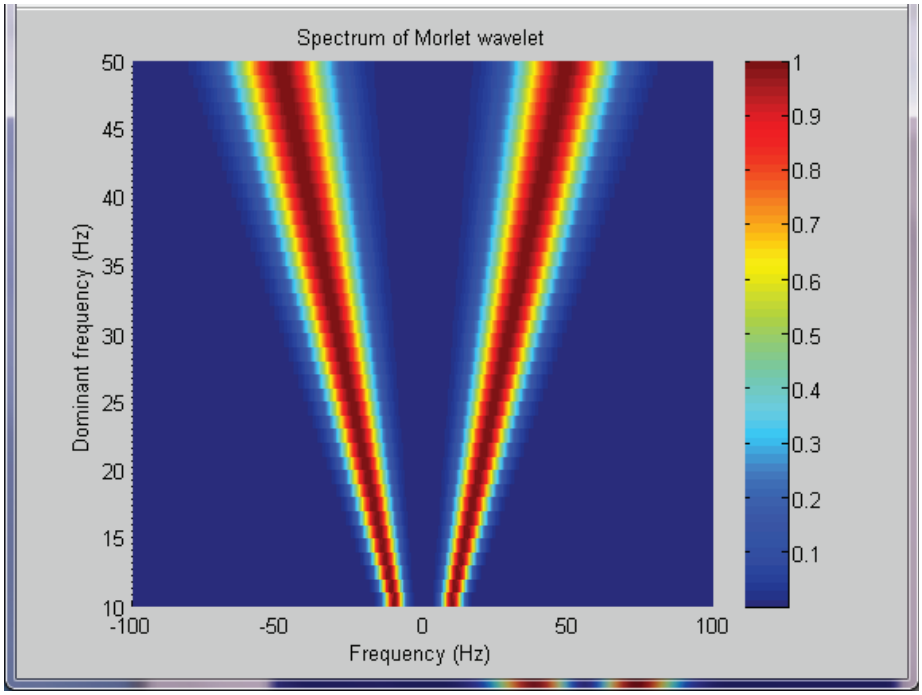

Figure D.4: Morlet wavelets in frequency

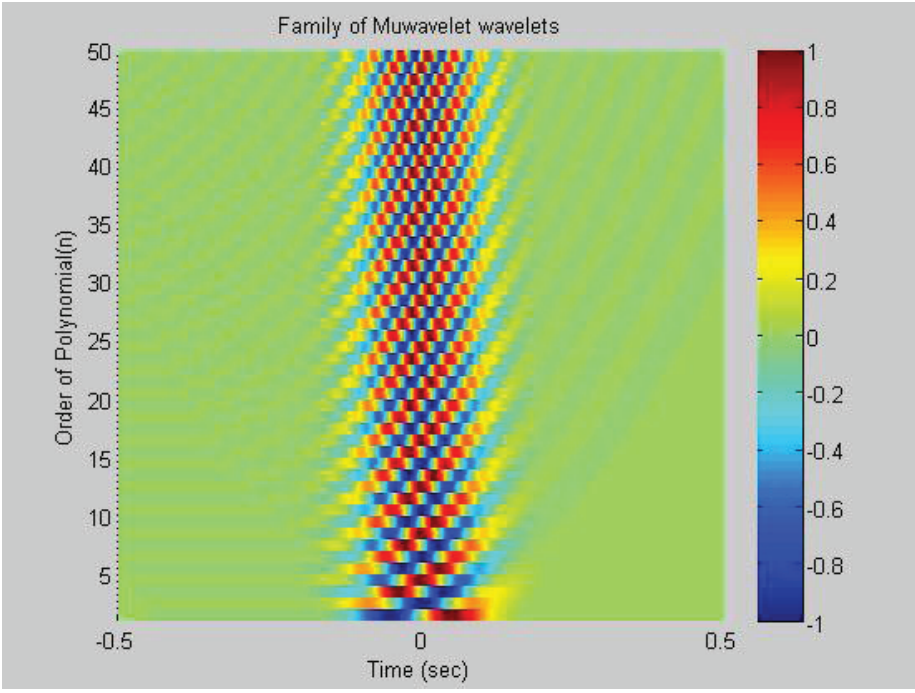

Figure D.5: μ wavelets in time

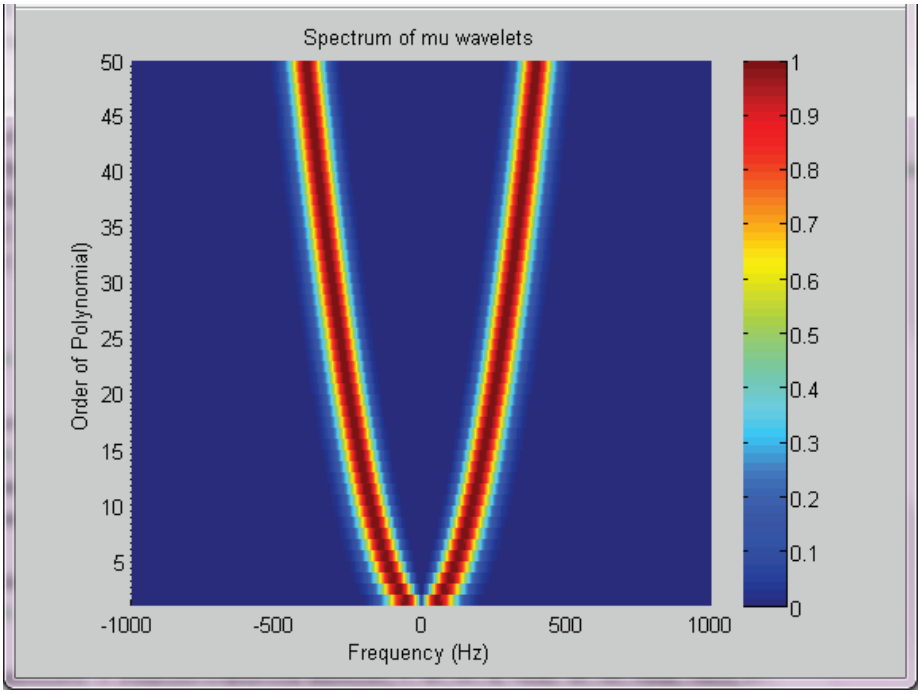

Figure D.6: μ wavelets in frequency

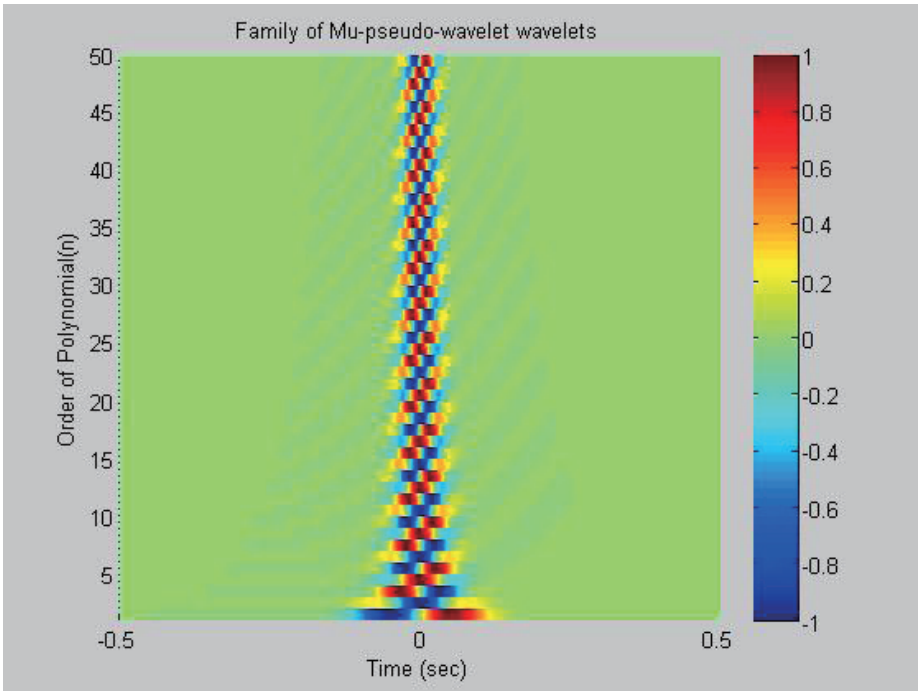

Figure D.7: Pseudo μ wavelets in time

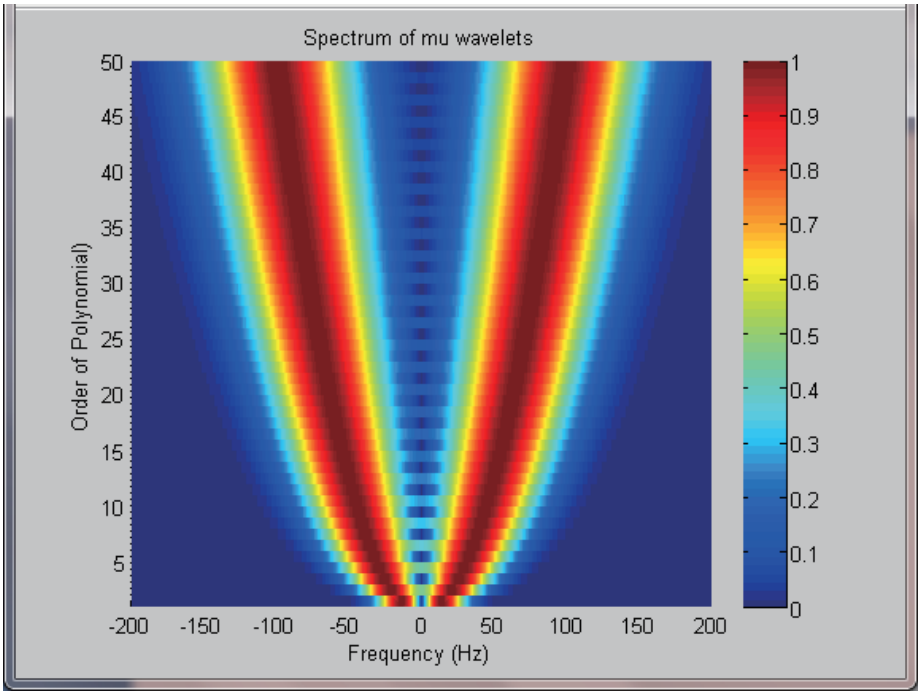

Figure D.8: Pseudo μ wavelets in frequency

Appendix E

Extra

E.1 Hermite μ and pseudo-μ

E.2 Wiggle plot of 30Hz Ricker wavelets at different phases

E.3 Spectral amplitude versus RC

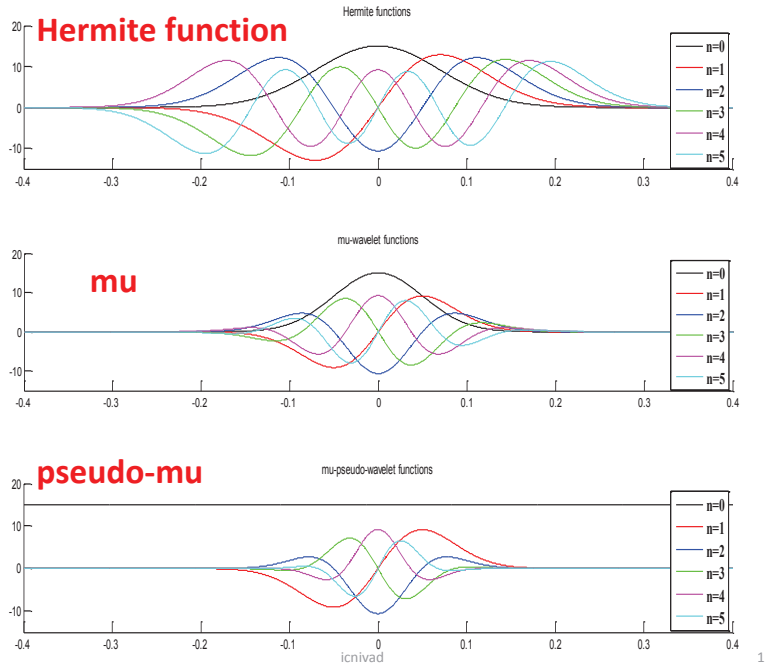

Figure E.1: First five orders of Hermite μ and pseudo-μ function

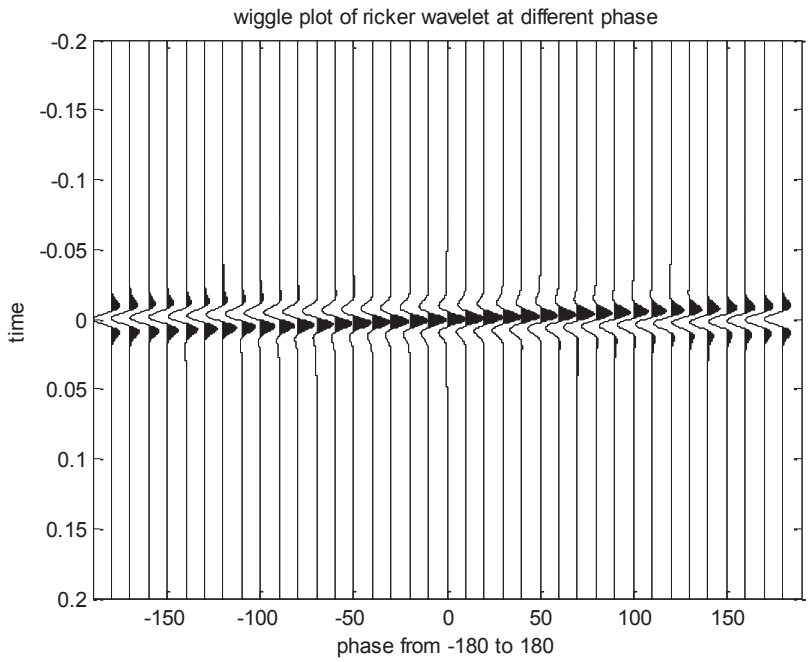

Figure E.2: Wiggle Plot of 30Hz Ricker wavelets at different phases

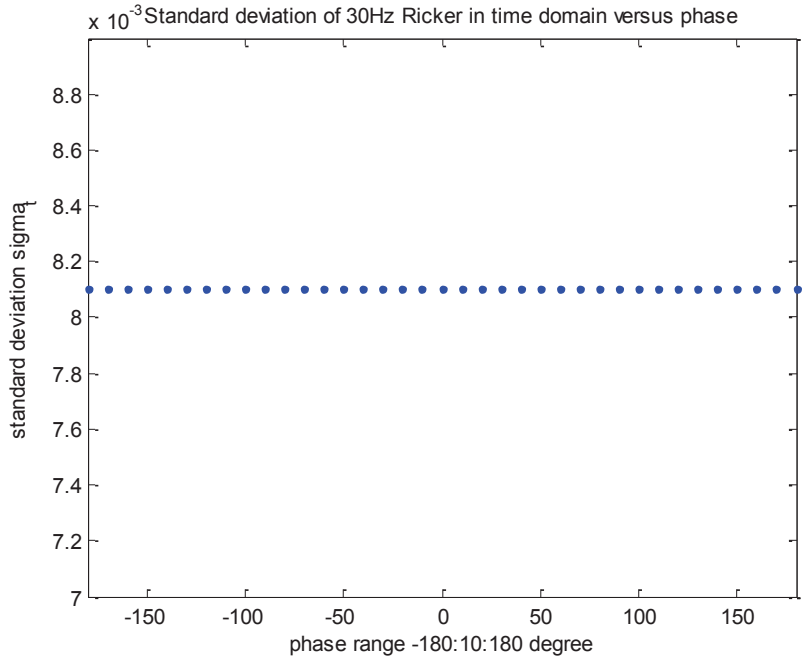

Figure E.3: σ_t of 30Hz Ricker wavelets versus phase/square UP

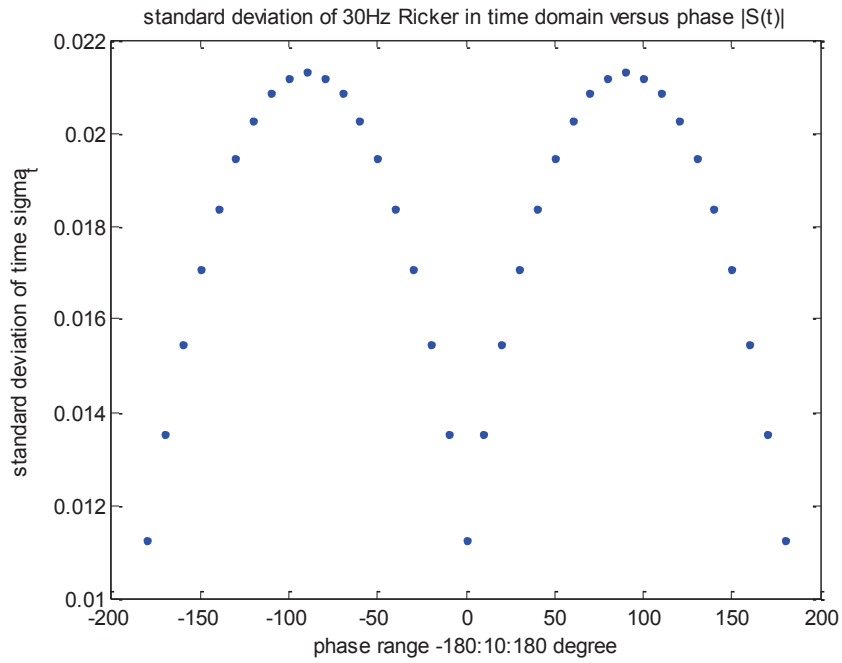

Figure E.4: σ_t of 30Hz Ricker wavelets versus phase/absolute UP

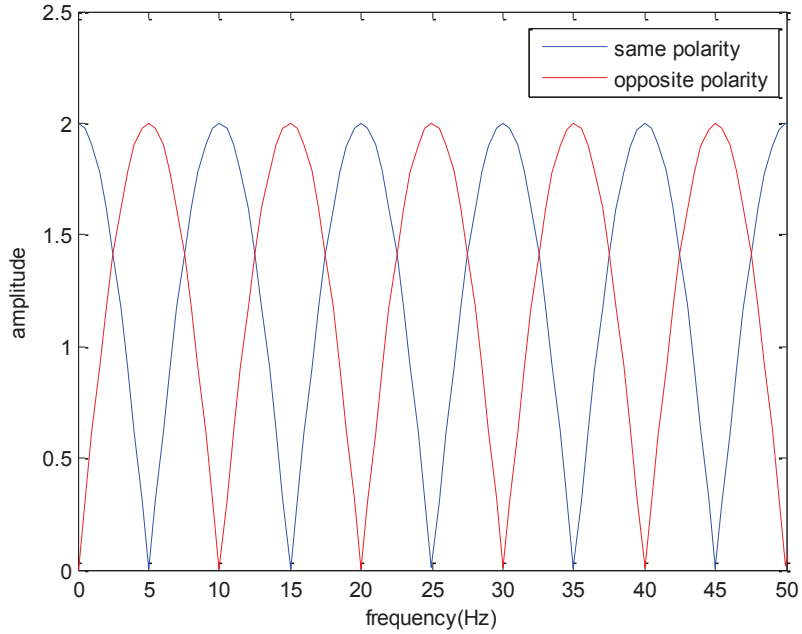

Figure E.5: Notches thickness relationship

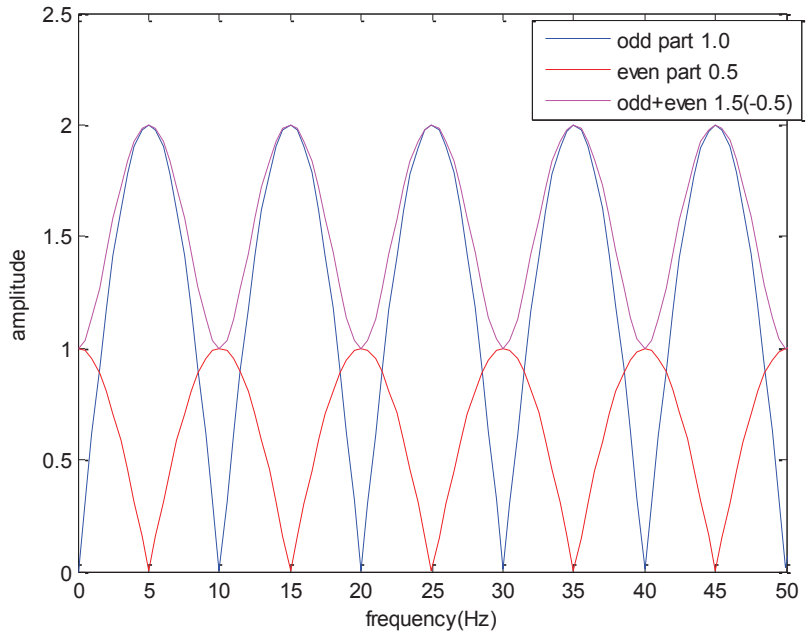

Figure E.6: Amplitude RC relationship 1

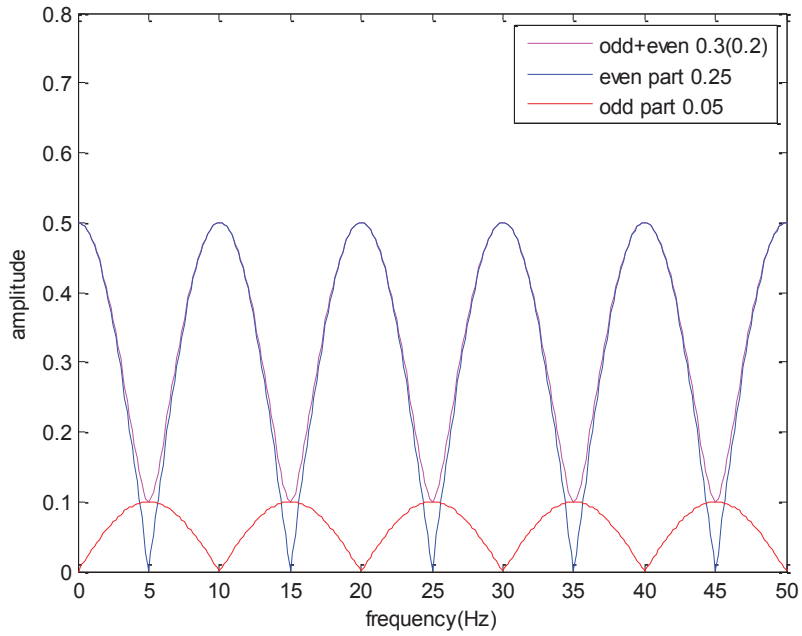

Figure E.7: Amplitude RC relationship 2

References

A. Alam and J. D. Taylor. Dip, azimuth and fault from continuous phase spectrum. *SEG Expanded Abstracts*, pages 998–1002, 2006.

A. E. Barnes, L. Fink, and K. Laughlin. Improving frequency domain thin bed analysis. *SEG Expanded Abstracts*, 23:1929–1932, 2004.

J. H. Bradford and Y. Wu. Instantaneous spectral analysis: Time-frequency mapping via wavelet matching with application to contaminated-site characterization by 3d gpr. *The Leading Edge*, pages 1018–1023, 2007.

M. D. Burnett, J. P. Castagna, E. Mendez-Hernandez, G. Z. Rodriguez, L. F. Garcia, J. T. M. Vazquez, M. T. Aviles, and R. V. Villasenor. Application of spectral decomposition to gas basins in mexico. *The Leading Edge*, pages 1130–1134, November 2003.

J. P. Castagna, S. Sun, and R. W. Siegfried. Instantaneous spectral analysis: Detection of low-frequency shadows associated with hydrocarbons. *The Leading Edge*, pages 120–127, February 2003.

A. Chakraborty and D. Okaya. Frequency-time decomposition of seismic data using wavelet-based methods. *Geophysics*, 60:1906–1916, 1995.

G. Chen, C. Finn, R. Neelamani, D. Gillard, G. Matteucci, and B. Fahmy. Spectral decomposition response to reservoir fluids from a deepwater reservoir. *SEG Extended Abstracts*, pages 1665–1669, 2006.

S. Chopra, J. P. Castagna, and O. Portniaguine. Thin-bed reflectivity inversion. *SEG Extended Abstracts*, pages 2057–2061, 2006.

S. Chopra, J. P. Castagna, Y. Xu, and R. Tonn. Thin-bed reflectivity inversion and seismic interpretation. *SEG Extended Abstracts*, pages 1923–1927, 2007.

S. Chopra, J. P. Castagna, and Y. Xu. Relative acoustic impedance application for thin-bed reflectivity inversion. *SEG Extended Abstracts*, pages 3554–3558, 2009.

H. Chung and D. C. Lawton. Frequency characteristics of seismic reflections from thin beds. *Canadian Journal Of Exploration Geophysics*, 31:32–37, 1995.

L. Cohen. *Time-Frequency Analysis*. Prentice Hall, 1994.

J. Cuesta, R. Perez, F. Hernandez, W. Carrasquel, R. Cabrera, C. Moreno, and J. P. Castagna. The use of seismic attributes and spectral decomposition to support the drilling plan of the uraco-bombal fields. *SEG Extended Abstracts*, pages 1845–1849, 2009.

I. Daubechies. *Ten Lectures on Wavelets*. CBMS-NSF Regional Conference Series in Applied Mathematics, 1990.

J. Deng, D. Han, J. Liu, and Q. Yao. Application of spectral decomposition to detect deepwater gas reservoir. *SEG Expanded Abstracts*, pages 1427–1431, 2007.

W. A. Fahmy, G. Matteucci, D. Butters, J. Zhang, and J. P. Castagna. Successful application of spectral decomposition technology toward drilling of a key offshore development well. *SEG Extended Abstracts*, pages 262–265, 2005.

J. Friedman, T. Hastie, and R. Tibshirani. Additive logistic regression: A statistical view of boosting. *The Annals of Statistics*, 28(3):337–374, 2000.

I. C. Geerdes and R. A. Young. Spectral decomposition of 3-d ground penetrating radar data from the norman landfill. *SEG Extended Abstracts*, pages 1081–1085, 2005.

L. Giroldi and F. Alegria. Using spectral decomposition to identify and characterize glacial valleys and fluvial channels within the carboniferous section in bolivia. *The Leading Edge*, pages 1152–1158, 2005.

J. Gridley and G. Partyka. Processing and interpretational aspects of spectral decomposition. *SEG Extended Abstracts*, 16:1055–1058, 1997.

H. Guo, K. J. Marfurt, and J. Liu. Principal component spectral analysis. *Geophysics*, 74:P35–P43, 2009.

W. Guo, Y. Pang, M. Rauch-Davies, and Y. Gang. Successful application of spectral decomposition technique to map deep gas reservoirs. *SEG Extended Abstracts*, pages 491–495, 2006.

D. Hernandez and J. P. Castagna. Stratigraphic detection and hydrocarbon detection in offshore gulf of mexico miocene sandstone reservoirs using spectral decomposition. *SEG Extended Abstracts*, 23:533–536, 2004.

P. Johann, G. Ragagnin, and M. Spinola. Spectral decomposition reveals geological hidden features in the amplitude maps from a deep water reservoir in the campos basin. *SEG Expanded Abstracts*, 22:1740–1743, 2003.

R. S. Kallweit and L. C. Wood. The limits of resolution of zero-phase wavelets. *Geophysics*, 47(7):1035–1046, 1982.

Y. Li and X. Zhang. Spectral decomposition using wigner-ville distribution with applications to carbonate reservoir characterization. *The Leading Edge*, pages 1050–1055, 2008.

Y. Li, J. Li, and X. Zheng. Channel system characterization using wigner-ville distribution-based spectral decomposition. *SEG Expanded Abstracts*, pages 1418–1422, 2010.

Y. Li, X. Zheng, and Y. Zhang. High-frequency anomalies in carbonate reservoir characterization using spectral decomposition. *Geophysics*, 76:V47–V57, 2011.

Q. Liao, D. Kouri, D. Nanda, and J. Castagna. Automatic first break detection by spectral decomposition using minimum uncertainty wavelets. *SEG Expanded Abstracts*, pages 1627–1631, 2011.

J. Liu and K. J. Marfurt. Instantaneous spectral attributes to detect channels. *Geophysics*, 72:P23–P31, 2007.

S. G. Mallat and Z. Zhang. Matching pursuit with time-frequency dictionaries. *IEEE Transactions on signal processing*, 41:3397–3415, 1993.

K. J. Marfurt and R. L. Kirlin. Narrow-band spectral analysis and thin-bed tuning. *Geophysics*, 66:1274–1283, 2001.

M. C. Matos and K. J. Marfurt. Brazilian deep water carbonate reservoir study using the wavelet transform teager-kaiser energy. *SEG Expanded Abstracts*, pages 1516–1520, 2008.

M. C. Matos, K. Zhang, K. J. Marfurt, and R. Slatt. Stratigraphic discontinuities mapped through joint time-frequency seismic phase unwrapping. *SEG Extended Abstracts*, pages 1087–1091, 2009.

X. Miao, D. Todorovic-Marinic, and T. Klatt. Enhancing seismic insight by spectral decomposition. *SEG Expanded Abstracts*, pages 1437–1441, 2007.

P. Montoya, R. Tatham, W. Fisher, R. Steel, and M. Hudec. Definition of depositional geological elements in deep-water minibasins of the gulf of mexico using spectral decomposition in depth domain. *SEG Expanded Abstracts*, pages 481–485, 2005.

E. Odebeatu, J. Zhang, M. Chapman, E. Liu, and X. Li. Application of spectral decomposition to detection of dispersion anomalies associated with gas saturation. *The Leading Edge*, pages 206–210, February 2006.

A. Ozbek, A. K. Ozdemir, and M. Vassallo. Interpolation by matching pursuit. *SEG Expanded Abstracts*, pages 3254–3258, 2009.

G. Partyka. Seismic thickness estimation: Three approaches, pros and cons. *SEG extended abstracts*, 20:503–506, 2001.

G. Partyka, J. Gridley, and J. Lopez. Interpretational applications of spectral decomposition in reservoir characterization. *The Leading Edge*, 18:353–360, 1999.

L. Peyton, R. Bottjer, and G. Partyka. Interpretation of incised valleys using new 3-d seismic techniques: A case history using spectral decomposition and coherency. *The Leading Edge*, pages 1294–1297, 1998.

S. K. Pokhriyal and S. Dotiwala. Spectral decomposition attribute: A useful tool for mapping fault pattern in offshore kutch basin of india. *SEG Extended Abstracts*, pages 865–869, 2007.

C. I. Puryear, S. Tai, J. P. Castagna, R. Masters, and F. Dwan. Comparison of frequency attributes from cwt and mpd spectral decompositions of a complex turbidite channel model. *SEG Expanded Abstracts*, pages 393–397, 2008.

J. Sierra, W. Marin, M. Bonilla, and H. Campos. Structural and stratigraphic interpretation using spectral decomposition: applications in deepwater settings. *SEG Extended Abstracts*, pages 1850–1854, 2009.

S. Singleton, M. T. Taner, and S. Treitel. Q estimation using gabor-morlet joint time-frequency analysis techniques. *SEG Extended Abstracts*, pages 1610–1614, 2006.

S. Sinha, P. S. Routh, P. D. Anno, and J. P. Castagna. Spectral decomposition of seismic data with continuous-wavelet transform. *Geophysics*, 70:P15–P25, 2005.

S. Sinha, P. Routh, and P. Anno. Instantaneous spectral attributes using scales in continuous-wavelet transform. *Geophysics*, 74:WA137–WA142, 2009.

R. Spitzer, U. Sattler, and P. Strauss. Spectral decomposition - a case study from the vienna basin. *SEG Extended Abstracts*, pages 841–845, 2007.

S. Tai, C. I. Puryear, and J. P. Castagna. Local frequency as a direct hydrocarbon indicator. *SEG Expanded Abstracts*, pages 2160–2164, 2009.

A. K. Verma, M. Pereira, B. R. Bharali, A. K. Khanna, and R. Dasgupta. Use of spectral decomposition in seismic interpretation for finding out fluvial channel sand body: A case study from upper assam shelf basin, india. *SEG Extended Abstracts*, pages 598–602, 2009.

Y. Wang. Seismic time-frequency spectral decomposition by matching pursuit. *Geophysics*, 72:V13–V20, 2007.

M. B. Widess. How thin is a thin bed? *Geophysics*, 38(6):1176–1180, 1973.

K. Zhang, K. J. Marfurt, R. M. Slatt, and Y. Guo. Spectral decomposition illumination of reservoir facies. *SEG Extended Abstracts*, pages 3515–3519, 2009.

B. Zhao, D. Johnston, and W. Gouveia. Spectral decomposition of 4d seismic data. *SEG Extended Abstracts*, pages 3235–3239, 2006.